Check for updates

The Causes of Leaf Hydraulic Vulnerability and Its Influence on Gas Exchange in *Arabidopsis thaliana*[1][OPEN]

Christine Scoffoni,[a,b,2,3] Caetano Albuquerque,[c] Hervé Cochard,[d] Thomas N. Buckley,[e] Leila R. Fletcher,[a] Marissa A. Caringella,[a] Megan Bartlett,[f] Craig R. Brodersen,[g] Steven Jansen,[h] Andrew J. McElrone,[c,i] and Lawren Sack[a]

[a]Department of Ecology and Evolutionary Biology, University of California, Los Angeles, California 90095
[b]Department of Biological Sciences, California State University, Los Angeles, California 90032
[c]Department of Viticulture and Enology, University of California, Davis, California 95616
[d]Université Clermont-Auvergne, Institut National de la Recherche Agronomique, PIAF, F-63000 Clermont-Ferrand, France
[e]Department of Plant Sciences, University of California, Davis, California 95616
[f]Princeton Environmental Institute, Princeton University, Princeton, New Jersey 08544
[g]School of Forestry and Environmental Studies, Yale University, New Haven, Connecticut 06511
[h]Institute of Systematic Botany and Ecology, Ulm University, Ulm, Germany 89081
[i]United States Department of Agriculture-Agricultural Research Service, Davis, California 95616

ORCID IDs: 0000-0002-2680-3608 (C.S.); 0000-0001-6222-3996 (C.A.); 0000-0002-2727-7072 (H.C.); 0000-0001-7610-7136 (T.N.B.); 0000-0002-2380-041X (L.R.F.); 0000-0002-0924-2570 (C.R.B.); 0000-0002-4476-5334 (S.J.); 0000-0002-7009-7202 (L.S.).

The influence of the dynamics of leaf hydraulic conductance (K_{leaf}) diurnally and during dehydration on stomatal conductance and photosynthesis remains unclear. Using the model species Arabidopsis (*Arabidopsis thaliana* ecotype Columbia-0), we applied a multitiered approach including physiological measurements, high-resolution x-ray microcomputed tomography, and modeling at a range of scales to characterize (1) K_{leaf} decline during dehydration; (2) its basis in the hydraulic conductances of leaf xylem and outside-xylem pathways (K_{ox}); (3) the dependence of its dynamics on irradiance; (4) its impact on diurnal patterns of stomatal conductance and photosynthetic rate; and (5) its influence on gas exchange and survival under simulated drought regimes. Arabidopsis leaves showed strong vulnerability to dehydration diurnally in both gas exchange and hydraulic conductance, despite lack of xylem embolism or conduit collapse above the turgor loss point, indicating a pronounced sensitivity of K_{ox} to dehydration. K_{leaf} increased under higher irradiance in well-hydrated leaves across the full range of water potential, but no shift in K_{leaf} vulnerability was observed. Modeling indicated that responses to dehydration and irradiance are likely attributable to changes in membrane permeability and that a dynamic K_{ox} would contribute strongly to stomatal closure, improving performance, survival, and efficient water use during drought. These findings for Columbia-0 provide a baseline for assessing variation across genotypes in hydraulic traits and their influence on gas exchange during dehydration.

Plant growth requires a copious water supply because the rate of CO_2 uptake for photosynthesis depends on stomatal conductance (g_s), which results in transpiratory water loss. Because stomata close in dehydrating leaves, photosynthesis and growth depend on the efficiency of water replacement to the mesophyll. Thus, in the past two decades, many studies focusing on diverse species have shown the centrality of the plant hydraulic system in determining leaf-scale gas exchange and plant productivity (Sack and Holbrook, 2006; Brodribb et al., 2007; Scoffoni et al., 2016). Our aim was to test hypotheses for the dynamics of hydraulic traits and their influence on gas exchange during dehydration using the model species *Arabidopsis thaliana* (further referred to as Arabidopsis). Establishing a framework for testing the influence of hydraulic traits in Arabidopsis can help address recent debates and open avenues for the discovery of genetic associations

[1] This work was supported by the U.S. National Science Foundation (award nos. 1457279 and 1557906), a Humboldt Research Postdoctoral Fellowship, a CAPES/Brazil Fellowship, and the International Wheat Yield Partnership. The Advanced Light Source is supported by the Director, Office of Science, Office of Basic Energy Sciences, of the U.S. Department of Energy (contract no. DE-AC02-05CH11231).

[2] Author for contact: cscoffo@calstatela.edu.
[3] Senior author.
The author responsible for distribution of materials integral to the findings presented in this article in accordance with the policy described in the Instructions for Authors (www.plantphysiol.org) is: Christine Scoffoni (cscoffo@calstatela.edu).

C.S. and L.S. designed the study; C.S., C.A., H.C., T.N.B., L.R.F., M.A.C., M.B., A.J.M., and L.S. contributed to data collection and/or analyses; C.S. and L.S. wrote the article with input from all authors.
[OPEN] Articles can be viewed without a subscription.
www.plantphysiol.org/cgi/doi/10.1104/pp.18.00743

 © 2018 American Society of Plant Biologists. All Rights Reserved.

Downloaded from https://academic.oup.com/plphys/article/178/4/1584/6116813 by University of California, San Francisco user on 29 November 2022

in natural and mutant genotypes under moist conditions and during soil and/or atmospheric drought.

The leaf accounts for a large proportion of plant hydraulic resistance (Sack and Holbrook, 2006). Thus, theoretical and empirical studies have shown strong correlations of g_s and photosynthetic rate (A_{max}) with leaf hydraulic conductance (K_{leaf}; determined as the flow rate divided by the water potential driving force, in units of mmol m^{-2} s^{-1} MPa^{-1}) across species under well-watered conditions (Nardini and Salleo, 2003; Brodribb and Holbrook, 2004; Sack and Holbrook, 2006; Scoffoni et al., 2016) and within given species during dehydration (Brodribb and Holbrook, 2006, 2007; Bartlett et al., 2016; Scoffoni et al., 2017c). A high K_{leaf} enabling higher g_s and A_{max} could be achieved through a high vein length per area, larger and/or more numerous xylem conduits (and/or xylem pits), and more conductive mesophyll and bundle sheath anatomy and biochemistry (Brodribb et al., 2007; Choat et al., 2008; Caringella et al., 2015; Scoffoni et al., 2015, 2016; Stewart et al., 2018). Yet, the linkages of K_{leaf} and gas exchange as leaves dehydrate to the turgor loss point are still under debate. Early studies suggested that K_{leaf} decline drives stomatal closure under high vapor pressure deficits (VPDs) at midday (Brodribb and Holbrook, 2003a; Bucci et al., 2003) and during drought (Salleo et al., 2001; Brodribb and Holbrook, 2003b; Nardini and Salleo, 2003). Several recent studies suggested that, in some species, K_{leaf} might not decline until embolism forms in the leaf vein xylem (Brodribb et al., 2016a, 2016b; Skelton et al., 2017), which for many species does not occur until past the point of stomatal closure and bulk leaf turgor loss (Brodribb et al., 2016b; Hochberg et al., 2017; Scoffoni et al., 2017a). Similarly, xylem wall collapse may drive K_{leaf} declines in pine (*Pinus* spp.) needles and minor veins of *Quercus rubra* (red oak) only below the turgor loss point (Cochard et al., 2004a; Zhang et al., 2016). Avoiding K_{leaf} decline during transpiration when leaves are hydrated above the turgor loss point has been suggested as adaptive, maintaining leaf water potential (Ψ_{leaf}) and open stomata, although at the risk of sustaining water potentials that would induce xylem cavitation under high VPDs (Brodribb and Holbrook, 2006). Numerous studies in the last decade have shown that species differ in whether K_{leaf} declines at milder, similar, or more severe Ψ_{leaf} than at stomatal closure and that K_{leaf} decline depends mechanistically on processes in multiple tissues: the venation, bundle sheath, and mesophyll pathways of liquid and vapor transport (for review, see Scoffoni et al., 2017c). Indeed, a meta-analysis of the literature found that, on average, across species (and methods for K_{leaf} determination), K_{leaf} declined by 30% to 80% before the turgor loss point (Scoffoni et al., 2017c). Recent work focusing on partitioning leaf xylem and outside-xylem resistances during dehydration suggested the outside-xylem hydraulic conductance (K_{ox}) as the primary driver of K_{leaf} decline (Trifiló et al., 2016; Scoffoni et al., 2017a, 2017c), which could be triggered by the loss of cell connectivity, cell shrinkage, and/or changes in membrane aquaporin activity (Laur and Hacke, 2014b; Scoffoni et al., 2014, 2017a), potentially mediated by the effects of abscisic acid (ABA) in the bundle sheath (Pantin et al., 2013). A recent study in rice (*Oryza sativa*) has attributed to K_{leaf} decline a strong causal role in driving stomatal closure during dehydration (Wang et al., 2018).

Debate has also focused on the light response of K_{leaf}. Previous studies have found many species to exhibit a rapid enhancement of K_{leaf} in response to increased irradiance (Sack et al., 2002; Nardini et al., 2005b; Tyree et al., 2005; Cochard et al., 2007; Scoffoni et al., 2008; Voicu et al., 2008; Guyot et al., 2012; Xiong et al., 2018), but not all (Sack et al., 2002; Gasco et al., 2004; Tyree et al., 2005; Scoffoni et al., 2008; Xiong et al., 2018). The activation of $PIP_{2,1}$ and $PIP_{2,2}$ aquaporins under high irradiance at high water potential has been shown to also enhance K_{leaf} in some (Cochard et al., 2007) though not all species (Voicu et al., 2009). A higher K_{leaf} under high light could potentially help buffer rapid changes in VPD and prevent stomata from closing (Carins Murphy et al., 2012; Scoffoni et al., 2015). In Arabidopsis, one study estimated hydraulic conductance by pushing water into entire rosettes suspended underwater in a dark pressure chamber and found that it was higher for leaves acclimated to dark rather than high irradiance (Prado et al., 2013), although no study has investigated this response at the leaf level.

Here, we applied complementary physiological, imaging, and modeling approaches (Table 1) to assess K_{leaf} dynamics with dehydration and irradiance and their role in driving diurnal patterns of gas exchange in Arabidopsis. We tested the hypotheses in Arabidopsis that K_{leaf} (1) is high under well-hydrated conditions but declines strongly during dehydration; (2) declines due to changes in K_{ox} but not in xylem embolism formation or conduit collapse; (3) responds to irradiance; (4) influences diurnal patterns of g_s and photosynthetic rate; and (5) shows dynamics that confer higher water-use efficiency and, thus, that would benefit plant performance under simulated soil drying.

RESULTS

Leaf Hydraulics and Gas Exchange and Their Responses to Leaf Dehydration and Irradiance in Arabidopsis

Arabidopsis Col-0 exhibited high maximum K_{leaf}, g_s, g_{min}, as well as A_{area} (Figs. 1 and 2; Table 2). The partitioning of hydraulic resistances in the leaf indicated a similar distribution of resistances in the xylem and outside-xylem pathways (45.6% versus 54.4% respectively; Table 2).

Arabidopsis showed a strong vulnerability to dehydration in K_{leaf} and gas exchange (Fig. 1). Notably, the range of water potential measured on intact plants diurnally, and on detached leaves during bench dehydration, was similar (Figs. 1 and 2). K_{leaf} responded nonlinearly to dehydration, with steep declines before

Downloaded from https://academic.oup.com/plphys/article/178/4/1584/6116813 by University of California, San Francisco user on 29 November 2022

Table 1. *Modeling framework across scales to determine the underlying mechanisms linking K_{leaf} decline to gas exchange*

A_{area}, Leaf photosynthetic rate; g_{max}, maximum stomatal conductance; g_{min}, minimum epidermal conductance; K_x, leaf xylem hydraulic conductance; PLC, percentage loss of hydraulic conductance.

Model	Purpose	Input	Output	Results
K_LEAF (Cochard et al., 2004; Scoffoni et al., 2017a)	Model the influence of xylem embolism and potential conduit collapse on K_x and K_{leaf}	Leaf size, number of secondary veins, and theoretical conductivities from the different vein orders (1) at full turgor and after accounting (2) for the decline caused by the observed embolism in midrib and/or secondary veins and (3) for the decline potentially caused by collapsed xylem conduits of tertiary and higher order veins (under a realistic collapsed scenario as observed in red oak species [Zhang et al., 2016], which caused 13% PLC, and a more severe scenario causing 50% PLC)	K_x	Neither embolism nor xylem conduit collapse caused a decline in K_x substantial enough to explain the observed decline in K_{leaf}
MOFLO 2.0 (Buckley et al., 2017)	Model the influence of changes in outside-xylem pathways on K_{ox} and K_{leaf}	Cell shrinkage and percentage intercellular airspace at −0.5 MPa obtained from microCT, g_s (abaxial and adaxial), VPD, and bulk leaf temperature; simulations were performed under no light or 600 μmol m^{-2} s^{-1} photosynthetically active radiation, with or without an apoplastic barrier at the bundle sheath and with or without an 80% decline in cell membrane permeability and/or cell connectivity	K_{ox}	Reduction of cell membrane permeability in the context of an apoplastic barrier would account for most of the K_{leaf} decline observed at −0.5 MPa; temperature gradients through the leaf due to irradiance had little impact on K_{ox}
Marginal contribution of K decline (refined from Rodriguez-Dominguez et al., 2016)	Quantify the influence of K_{leaf} decline on g_s decline	Parameters from the maximum likelihood function of g_s and K_{leaf} versus Ψ_{leaf}, VPD set at a constant value (1.5 kPa), and a computed range of percentage g_s decline (0%–100% decline in g_s with Ψ_{leaf})	Contribution of K_{leaf} decline to g_s decline with dehydration	K_{leaf} decline explains most of the changes in g_s during mild to moderate dehydration
SurEau (Martin-StPaul et al., 2017)	Quantify the influence of K_{leaf} decline on gas exchange in the whole-plant context during drought	Parameters from the maximum likelihood function of K_{leaf} versus Ψ_{leaf}, parameters from the function of K_{root} versus water potential, g_{min}, g_{max}, Farquhar's model inputs, photosynthetically active radiation, air temperature, air humidity, time of day, transpiration under well-hydrated conditions, and soil volume	Soil water reserve, water potentials, transpiration rate, g_s, A_{area}, and PLC	Decline in K_{leaf} causes Ψ_{leaf} to drop, which in turn causes both g_s and A_{area} to decline under increasing VPD and decreasing soil water potential

50% loss of its initial K_{leaf} by −0.17 MPa (K_{leaf} P_{50}) and gradually slowing down its response to further dehydration (Table 2; Fig. 1). Both g_s and A_{area} responded linearly to declining Ψ_{leaf} (Fig. 2), reaching 50% loss of initial rates by −0.37 and −0.38 MPa, respectively, and 95% loss at similar Ψ_{leaf} values of −0.71 MPa (Table 2). At the turgor loss point, K_{leaf} had declined by approximately 88% and stomata were nearly fully closed (Table 2; Fig. 1).

Leaves acclimated to high irradiance had significantly higher K_{leaf} values than leaves acclimated to low irradiance, with a 60% enhancement of K_{leaf} from low to high irradiance in well-hydrated leaves of Col-0 (Fig. 1). Student's t test was done on residuals of K_{leaf} (i.e. difference of observed values relative to those predicted from the best fit function through all data combined: $[K_{leaf} = 8.33 + 83.7 \times \exp(-(9.47 \times \Psi_{leaf}))]$). Residuals for K_{leaf} were 7.4 mmol m^{-2} s^{-1} MPa^{-1} higher under high

Downloaded from https://academic.oup.com/plphys/article/178/4/1584/6116813 by University of California, San Francisco user on 29 November 2022

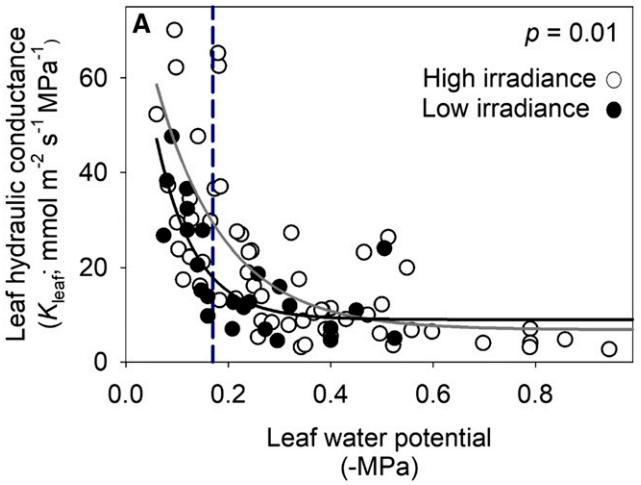

Figure 1. Decline of K_{leaf} measured under high (greater than 1,000 μmol photons m^{-2} s^{-1}) or low (less than 3 μmol photons m^{-2} s^{-1}) irradiance. The maximum likelihood function is shown for K_{leaf} vulnerability acclimated under high light ($K_{leaf} = 6.83 + 81.4\exp(-7.56 \times |\Psi_{leaf}|)$) and low light ($K_{leaf} = 8.98 + 84.2\exp(-13.2 \times |\Psi_{leaf}|)$). The dashed line represents the water potential at 50% loss of K_{leaf} (similar in both treatments).

irradiance across the entire vulnerability curve ($P = 0.01$), 7.9 mmol m^{-2} s^{-1} MPa^{-1} higher considering only leaves above the turgor loss point ($P = 0.01$), and 13.9 mmol m^{-2} s^{-1} MPa^{-1} higher considering only leaves at hydration above −0.2 MPa ($P = 0.04$). However, leaves acclimated to high and low irradiance were similar in their K_{leaf} P_{50} (−0.17 versus −0.16 MPa, respectively; Fig. 1).

Diurnal Responses of Gas Exchange

Photosynthetic and stomatal responses were measured over the course of 2 d, from 09:00 to 18:00. Our results showed that the diurnal pattern of K_{plant} and gas exchange reflected the dynamics of Ψ_{leaf}, as evidenced by the strong trends of K_{plant}, g_s, and A_{max} versus Ψ_{leaf} ($r^2 = 0.45$–0.81, $P < 0.02$; Fig. 2). Of all the potential environmental drivers, VPD most strongly correlated with g_s dynamics diurnally ($r^2 = 0.18$, $P = 0.002$; Supplemental Fig. S1).

Independent effects analysis of potential drivers of diurnal dynamics in g_s, including environmental factors and Ψ_{leaf}, showed that Ψ_{leaf} was the most important statistically, contributing 77% toward the diurnal variation (Supplemental Fig. S2). The VPD contributed 11%, and temperature, photosynthetically active radiation, and time of day each contributed only 4% to the observed variation (Supplemental Fig. S2).

Testing for Vein Xylem Embolism and Collapse during Leaf Dehydration Using Microcomputed Tomography

We scanned leaves using in vivo microcomputed tomography (microCT) for dehydrated plants to visualize potential xylem embolism. In 14 of 18 leaves attached to plants that spanned the observed range of Ψ_{leaf} (−0.05 to −0.87 MPa), no gas embolism was observed in major or minor veins (Fig. 3). In four of 18 scans, we observed one to two embolized conduits in the midrib and/or secondary veins; notably, these leaves were not the most dehydrated (Ψ_{leaf} = −0.13 to −0.45 MPa; Fig. 4; Table 3) but were within the same range as other leaves that did not exhibit embolism. In all three leaves that showed embolized midrib conduits, the embolism spanned the entire length of the scanned section, and we were unable to measure the total vessel length (Fig. 4; Table 3). For two leaves, the embolized midrib

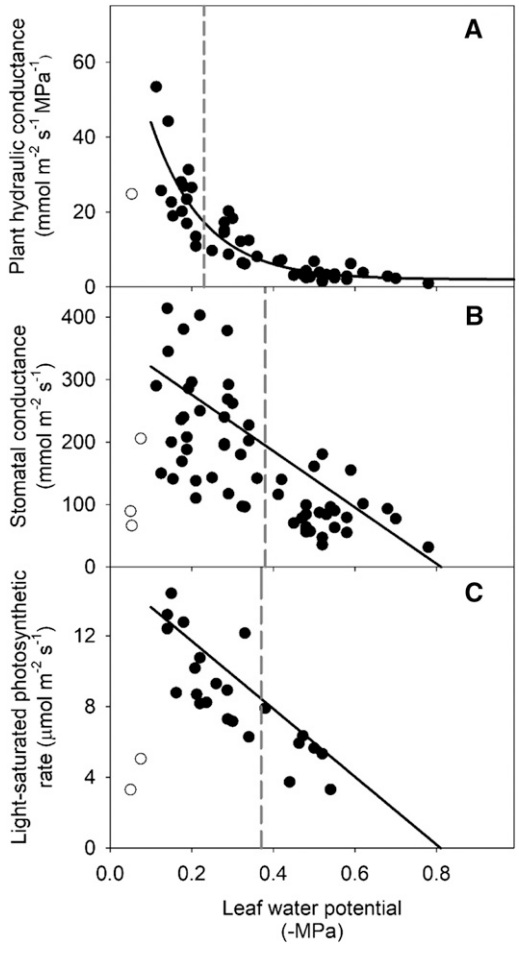

Figure 2. Plant hydraulic and gas-exchange responses to dehydration in Arabidopsis. Decline of the whole-plant hydraulic conductance (K_{plant}; A), g_s (B), and A_{area} (C) with dehydration are shown. Each point represents a different measured leaf. K_{plant} was obtained from the porometer data by dividing transpiration by Ψ_{leaf} (assuming that soil water potential was at full saturation). The black fitted line in each graph is the maximum likelihood function [exponential for $K_{plant} = 2.0 + 91.1\exp(-7.75 \times |\Psi_{leaf}|)$ and linear for $g_s = 339 - 451 \times |\Psi_{leaf}|$ and $A_{area} = 14.4 - 19.2 \times |\Psi_{leaf}|$]. The dotted gray line is the Ψ_{leaf} at 50% loss of maximum K_{plant}, g_s, or A_{area}. Because trait values above −0.1 MPa were especially low (white circles), likely representing stomatal closure at those high water potentials (see "Materials and Methods"), we did not include these points in the line fitting.

Downloaded from https://academic.oup.com/plphys/article/178/4/1584/6116813 by University of California, San Francisco user on 29 November 2022

Table 2. *Mean ± SE for the physiological and anatomical traits measured for Arabidopsis (Col-0)*

K_{max}, Maximum leaf hydraulic conductance; $\%R_{ox}$, percentage resistance outside the leaf xylem; P_{50}, P_{88}, and P_{95}, Ψ_{leaf} at 50%, 88%, and 95% decline in a given trait. %Rleaf, percentage leaf hydraulic resistance; Kt, theoretical hydraulic conductance.

Trait	Units	Col-0
Hydraulics and gas exchange		
K_{max}	mmol m^{-2} s^{-1} MPa^{-1}	59.9 ± 1.76
$K_{leaf0.1\text{-}0.2MPa}$	mmol m^{-2} s^{-1} MPa^{-1}	33.1 ± 4.55
K_x	mmol m^{-2} s^{-1} MPa^{-1}	138.4 ± 14.5
K_{ox}	mmol m^{-2} s^{-1} MPa^{-1}	106
$\%R_{ox}$	%	54.4
$\%R_{leaf}$	%	85.7
g_s	mmol m^{-2} s^{-1}	339 ± 24.9
A_{max}	μmol m^{-2} s^{-1}	14.4 ± 2.72
K_{leaf} P_{50}	MPa	−0.17
g_s P_{50}	MPa	−0.38
A_{area} P_{50}	MPa	−0.37
K_{leaf} P_{88}	MPa	−0.72
g_s P_{95}	MPa	−0.71
A_{area} P_{95}	MPa	−0.71
Drought tolerance traits		
Turgor loss point	MPa	−0.73
Osmotic potential at full turgor	MPa	−0.63
Modulus of elasticity	MPa	5.70
Relative water content at the turgor loss point	%	84.1
Leaf mass per unit of leaf area	g m^{-2}	13.6 ± 0.89
Percentage loss of area in a dry leaf	%	57.9 ± 3.05
g_{min}	mmol m^{-2} s^{-1}	18.6 ± 1.33
Leaf anatomical traits		
Distance from vein to lower epidermis	mm	0.067 ± 0.002
Total vein length per area	mm mm^{-2}	3.04 ± 0.08
Minor vein length per area	mm mm^{-2}	1.79 ± 0.08
Major vein length per area	mm mm^{-2}	1.25 ± 0.05
K_t, midrib per leaf area	mmol m^{-1} s^{-1} MPa^{-1}	0.27 ± 0.12
K_t, minor per leaf area	mmol m^{-1} s^{-1} MPa^{-1}	0.003 ± 0.0008

conduit extended into a secondary vein. In the fourth leaf, an isolated embolized conduit in the secondary vein was observed (Fig. 4; Table 3). All embolized conduits were of average diameter (Table 3; midrib conduit diameters measured under light microscopy ranged from 2.79 to 10.3 μm). No collapsed conduits were observed in midrib and secondary vein conduits at the range of water potentials investigated. The resolution of the microCT scans was not sufficient to determine whether conduit collapse occurred in higher order veins.

Modeling the Impact of Embolism and Collapse on Leaf Xylem Hydraulic Conductance

Spatially explicit modeling of the leaf xylem (Table 1) showed that the very low level of observed xylem conduit embolism would reduce K_x by 1.2% to 4.7% (Table 3). Because resolution was not sufficient to determine whether conduit collapse occurred in higher order veins, we simulated the potential impact of such a collapse if it had occurred. These simulations showed that, if higher order veins were to collapse to the same percentage of conduit diameter as reported recently for minor veins of *Quercus rubra* (Zhang et al., 2016), this would decrease K_x by 3% to 7.5% (Table 3). Under a more extreme scenario, in which the collapse of tertiary and minor veins caused a 50% decline in their conductivity, K_x would be reduced by 12% to 17% (Table 3), which would decrease K_{leaf} by 7% to 9%.

Modeling the Putative Causes of K_{ox} Decline

Spatially explicit modeling of the outside-xylem pathways using MOFLO 2.0 (Table 1) suggested that the main factor accounting for the decline in K_{ox} observed at −0.5 MPa was most likely the reduction of cell membrane permeability in combination with an apoplastic barrier at the bundle sheath (Fig. 5). Under high irradiance, an 80% reduction of cell membrane permeability would cause a 68.4% decrease in K_{ox}; adding an 80% reduction in cell connectivity would further decrease K_{ox} by 0.2% (Fig. 5). When performing these simulations with no apoplastic barrier at the bundle sheath, the impact of an 80% reduction of cell membrane permeability caused only a 24.5% decrease in K_{ox} (Fig. 5). Simulating the impact of changes of temperature gradients due to light absorption changed the percentage loss of K_{ox} by 1% to 3% across simulations (Supplemental

Downloaded from https://academic.oup.com/plphys/article/178/4/1584/6116813 by University of California, San Francisco user on 29 November 2022

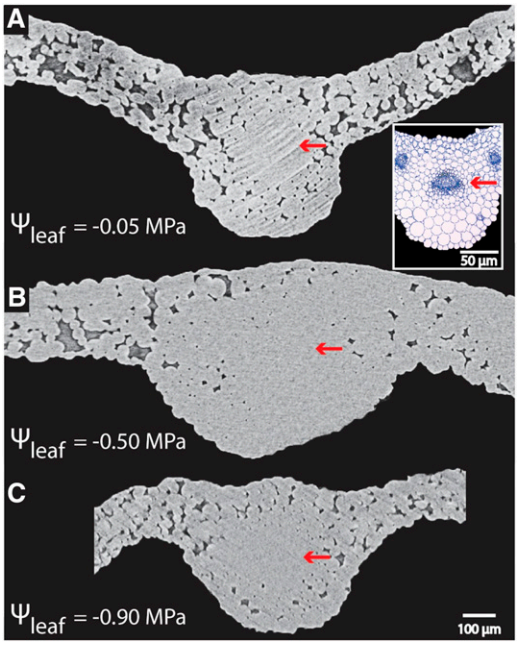

Figure 3. Lack of embolism observed in midrib conduits of Arabidopsis (Col-0) across levels of dehydration, as revealed by in vivo images of leaf midribs subjected to progressive dehydration using microCT. Water-filled cells appear in light gray in microCT. If air-filled (i.e. embolized) conduits were present, they would appear as black in the xylem portion of the midrib. There was no embolism, as shown in these images by the red arrows pointing at the entirely light gray midrib xylem. The Ψ_{leaf} has been provided for each image. The inset in A represents a leaf midrib cross section imaged under light microscopy, with the red arrow pointing to the xylem tissue (dark blue conduits).

Table S1). Finally, simulating the impact of cell shrinkage from full turgor to −0.5 MPa resulted in an increase in K_{ox} by 7% to 15%, due to the increase in vein density caused by leaf shrinkage and the consequent decrease in outside-xylem water flow path lengths (Fig. 5).

Partitioning the Contribution of K_{leaf} Vulnerability to g_s Decline

In a transpiring leaf, a low Ψ_{leaf} would result from low water potentials proximal to the leaf (i.e. in the soil or roots; Table 1) and to the transpiration-driven water potential drop across the leaf, which is greater, given K_{leaf} vulnerability. Thus, given that g_s declines with Ψ_{leaf}, K_{leaf} vulnerability will amplify the reduction of g_s at a given soil water potential and VPD. Using a partitioning analysis, we applied the observed parameters of g_s and K_{leaf} decline in Arabidopsis to compute the marginal percentage contribution of K_{leaf} vulnerability to the decline of g_s (Table 1). Our results showed that K_{leaf} vulnerability contributes strongly to g_s decline in transpiring leaves early in dehydration, due to the amplification of Ψ_{leaf} decline; when g_s declines by 30%, 70% of this response is due to K_{leaf} vulnerability rather than to low water potential proximal to the leaf (Fig. 6). The contribution of K_{leaf} vulnerability to g_s decline remains more than 40% until g_s declines by 50% and becomes less important as stomata approach full closure. When g_s has declined by 95%, the contribution of K_{leaf} vulnerability to g_s decline is less than 1%.

Using the SurEau Whole-Plant Physiology Model to Estimate the Influence of K_{leaf} Decline on Gas Exchange, Productivity, and Survival

We tested the importance of K_{leaf} vulnerability prior to the turgor loss point in reducing g_s and photosynthesis on plant carbon balance and survival in simulations using SurEau (Martin-StPaul et al., 2017; Fig. 7; Table 1). In simulations, the experimentally observed K_{leaf} vulnerability caused an up to −0.36-MPa lower Ψ_{leaf} at midday under well-hydrated conditions (yellow and red lines) compared with constant K_{leaf} simulations (light and dark blue lines; Fig. 7B). This lower Ψ_{leaf}, in turn, reduced g_s and cumulative CO_2 assimilation ($A_{n,\ tot}$) by up to 62% and 17%, respectively, under well-hydrated conditions (Fig. 7, A and B), but cumulative water-use efficiency (calculated as $A_{n,\ tot}$/total transpiration) increased by 28% (inset in Fig. 7C). Given finite soil water supply in these simulations, this higher water-use efficiency led to up to 24% higher $A_{n,\ tot}$ over the entire course of the simulated drought. Indeed, because K_{leaf} vulnerability results in lower g_s during the early stage of the drought, the soil water potential (approximated as nighttime Ψ_{leaf} in Fig. 7B) is maintained at higher levels as drought ensues, leading to the maintenance of higher g_s during later drought (Fig. 7A). Additionally, because Ψ_{leaf} does not drop as fast during the course of the drought, these simulations showed that, given K_{leaf} vulnerability, the onset of leaf xylem embolism occurs later during drought such that plants survive up to 6 d longer under drying soil (Fig. 7D). These simulations resulted in similar findings whether K_{root} was set as vulnerable or constant, highlighting K_{leaf} vulnerability as a main driver of improved water-use efficiency, $A_{n,\ tot}$, and survival during soil drying.

Drought Tolerance in Arabidopsis

Arabidopsis Col-0 exhibits low leaf mass per area, a high degree of area shrinkage during dehydration, high g_{min}, high osmotic potential at full turgor and the turgor loss point, and low modulus of elasticity and relative water content at the turgor loss point (Table 1).

DISCUSSION

Our results demonstrate a potential strong role for outside-xylem pathways in the decline of K_{leaf} with leaf dehydration, contributing to stomatal closure and the reduction of photosynthetic rate in Arabidopsis (Col-0). Strong declines in K_{leaf} were associated with declines in K_{plant}, g_s, and A_{area} at water potentials where no

Downloaded from https://academic.oup.com/plphys/article/178/4/1584/6116813 by University of California, San Francisco user on 29 November 2022

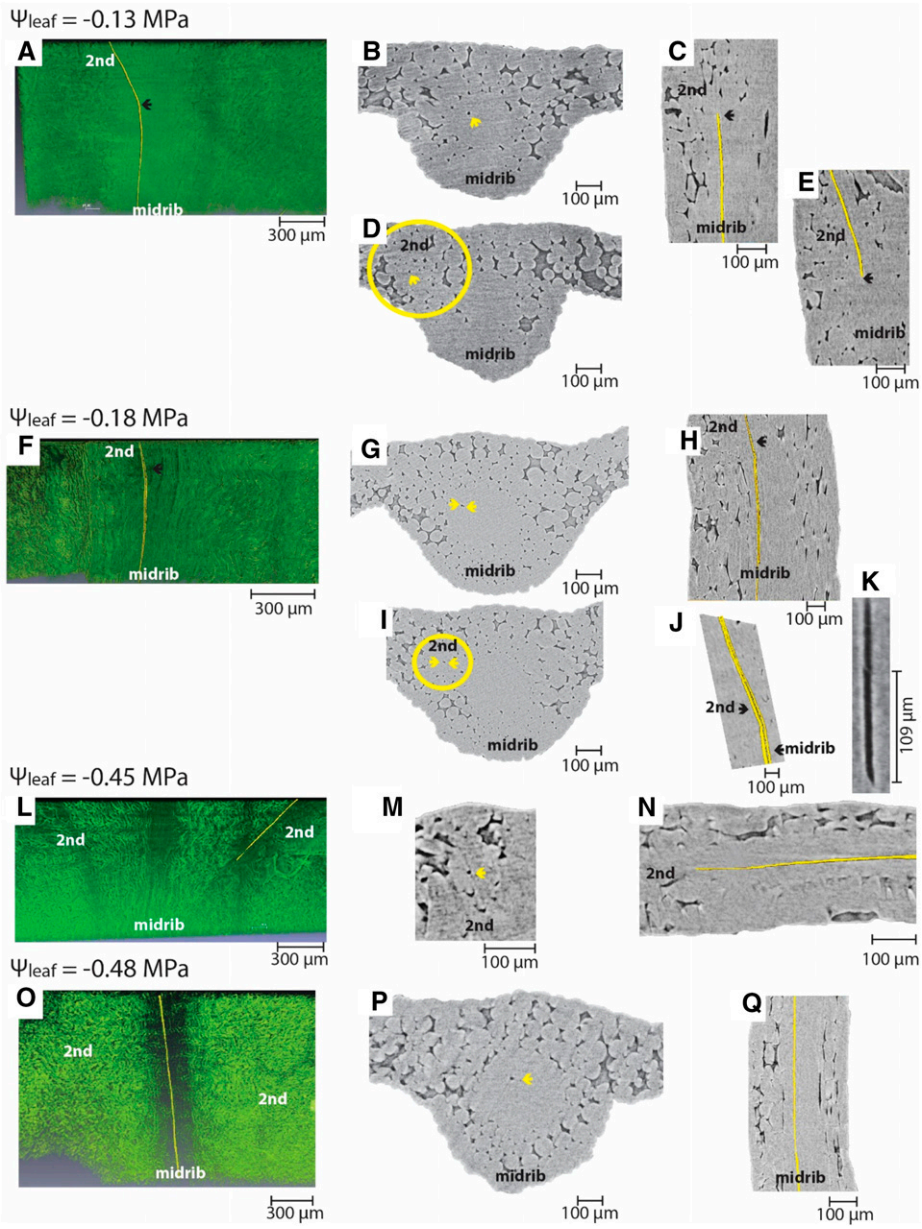

Figure 4. Rare embolisms were observed in a few individual leaves. In two samples, an embolized conduit was observed in the midrib; it continued into a secondary vein (A and F; the embolized conduits are depicted in yellow). The embolized conduit in the midrib and secondary vein can be seen in cross sections (B, D, G, and I) and longitudinal sections (C, E, H, and J) of the microCT scan. The arrows point to the embolized conduit (appearing as black in the microCT images). Because of the two dimensionalities of these sections, embolism in the midrib and secondary vein might appear disconnected (C and E). Note that, while the embolism was present in only one conduit per cross-sectional image, multiple conduits spanned the length of the midrib and secondary vein (as can be observed in K, where two conduits can be seen connected to one another). Most likely, a first conduit in the midrib embolized, and all the conduits connected directly to that one upstream embolized after. In one sample, an embolized conduit was observed isolated in the secondary vein (L–N), while in another sample, an embolized conduit was observed spanning the midrib length (O–Q).

significant embolism was observed using microCT. The absence of leaf xylem embolism before stomatal closure and hydraulic decline point to changes in outside-xylem pathways as the cause of the observed K_{leaf} decline and imply no functional role of xylem dysfunction in this species' response of gas exchange to leaf dehydration. Modeling showed that K_{leaf} vulnerability has a strong causal role in determining stomatal closure and, furthermore, that K_{leaf} vulnerability would improve plant carbon balance and survival during drought.

Drivers of K_{leaf} Decline during Dehydration

Our results suggest that changes in outside-xylem pathways are the main drivers of the response of K_{leaf} to dehydration in Arabidopsis. MicroCT imaging showed that embolism was rare in major vein xylem conduits and nonexistent in minor veins. Only one or two embolized conduits (representing on average 6%–11% of the conduits in the midrib) were found in four of 18 samples, with no trend of embolism with increasing water stress prior to the turgor loss point. This low vulnerability to embolism in leaves parallels findings for Arabidopsis inflorescence stems, which have P_{50} values lower than −2.5 MPa (Tixier et al., 2013). The few rare observed leaf vein xylem emboli likely arose from methodological artifacts. In three of the four samples in which embolized conduits were observed, the embolized conduit spanned the entire section. One possibility is that air may have entered the conduit when plants were removed from the soil for dehydration, if air entered conduits from damaged

Downloaded from https://academic.oup.com/plphys/article/178/4/1584/6116813 by University of California, San Francisco user on 29 November 2022

Table 3. *Observations of embolized conduits and dimensions from microCT and their simulated impact on* K_x *using the spatially explicit K_LEAF model*

Because we did not have the resolution to determine whether conduit collapse occurs in tertiary and minor veins, two simulations were performed based on minor vein conduit collapse observed in *Quercus rubra* (see "Materials and Methods"). Note that two leaves were imaged at each water potential (22 leaves total); embolism at the four water potentials below were only found in one of the two leaves tested at that water potential. Dashes are shown for samples where no embolized conduits were observed, and thus no simulations were performed.

Ψ_{leaf}	No. of Embolized Conduits			Length of Embolized Conduit	Diameter of Embolized Conduit		Simulated Percentage Loss of Xylem Hydraulic Conductance		
	Midrib	2°	3°+	Midrib	Midrib	2°	Embolism Only	Embolism + Realistic 3° + Vein Collapse (13% PLC)	Embolism + Severe 3° + Vein Collapse (50% PLC)
MPa				*μm*			%		
−0.06	0	0	0	–	–	–	0	–	–
−0.08	0	0	0	–	–	–	0	–	–
−0.13	1	1	0	>898	7.3	8.7	7.13	9.99	19.1
−0.16	0	0	0	–	–	–	0	–	–
−0.18	2	2	0	258, >600	6.2, 5.3	5.2, 3.5	3.96	6.70	16
−0.45	0	1	0	–	–	5.2	0.96	3.12	9.1
−0.48	1	0	0	>850	5.9	–	1.16	3.96	13
−0.50	0	0	0	–	–	–	0	–	–
−0.69	0	0	0	–	–	–	0	–	–
−0.79	0	0	0	–	–	–	0	–	–
−0.87	0	0	0	–	–	–	0	2.82	12

roots, and conduits were continuous into the major veins of scanned leaves. Similarly, air may have entered when the two leaves were excised from the plant for initial water potential measurement, if conduits spanned from these leaves to others in the rosette including the scanned leaves. Alternatively, these few embolisms could be the result of defects in the development of these conduits (Pickard, 1981; Tyree et al., 1994). Indeed, we found that a single isolated embolism event occurred in a secondary vein of one of our samples. Such isolated embolism events have been reported in leaf veins of other angiosperm species (Scoffoni et al., 2017b) and stem xylem (Brodersen et al., 2013; Choat et al., 2015, 2016).

MicroCT imaging did not reveal any conduit collapse in the midrib or secondary veins across the range of observed water potentials. Since the resolution of the microCT imaging did not permit the assessment of

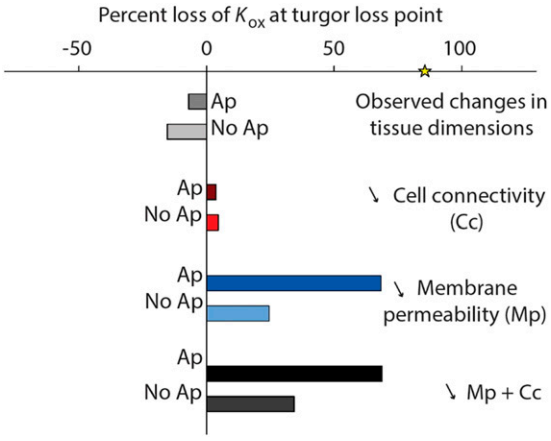

Figure 5. Results from simulations using a spatially explicit model of leaf outside-xylem water to test for potential drivers of the decline in K_{ox} in dehydrating leaf transport (MOFLO 2.0; Table 1; see "Materials and Methods"). The K_{ox} was first computed based on the decline of observed cell size and airspace alone (gray bars), which resulted in an increase in K_{ox} (negative percentage loss of K_{ox}; mainly due to the shortening of pathways from the veins to stomata). We then modeled the K_{ox} decline according to three scenarios (although always including the effect of tissue dimensional changes): an 80% decline at −0.5 MPa in (1) cell connectivity (red bars), (2) cell membrane permeability (blue bars), and (3) cell wall thickness (black bars). All simulations were run with (Ap; darker color) or without (No Ap; lighter color) an apoplastic barrier at the bundle sheath cells. The yellow star on the *x* axis represents the percentage observed K_{leaf} decline at −0.5 MPa (measured with the evaporative flux method; see "Materials and Methods").

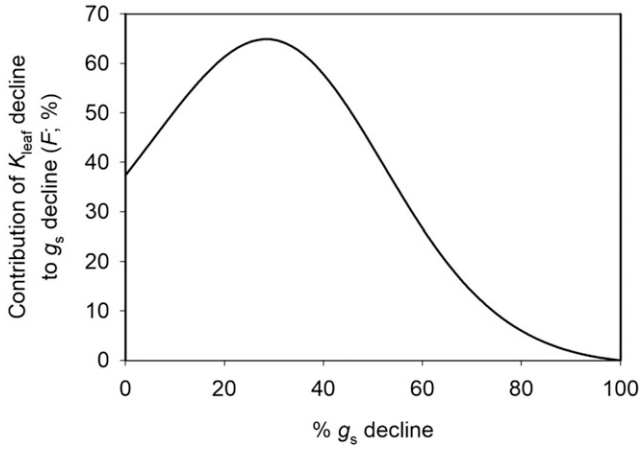

Figure 6. Model simulation mapping the contribution of the decline of K_{leaf} decline to that of g_s with dehydration (Table 1).

Downloaded from https://academic.oup.com/plphys/article/178/4/1584/6116813 by University of California, San Francisco user on 29 November 2022

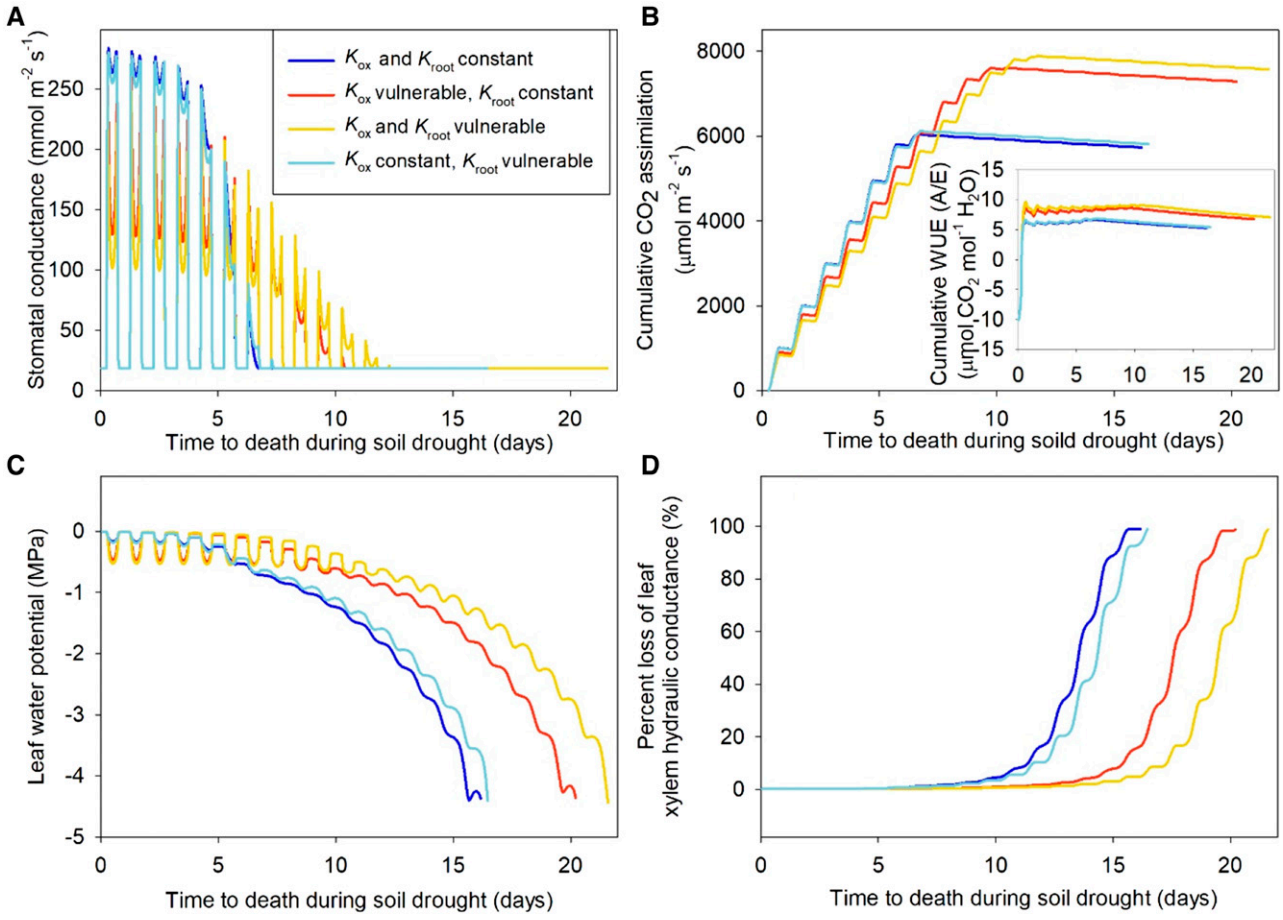

Figure 7. Daily simulated patterns of g_s (A), Ψ_{leaf} (B), $A_{n,\,tot}$ (C), and percentage loss of K_x (D) during the progression of a simulated soil drought (SurEau model; Table 1; see "Materials and Methods"). Four scenarios were modeled: (1) both K_{leaf} and root hydraulic conductance (K_{root}) were vulnerable to dehydration prior to the turgor loss point (yellow lines); (2) K_{leaf} was vulnerable but not K_{root} (red lines); (3) K_{root} was vulnerable but not K_{leaf} (light blue lines); or (4) neither K_{leaf} nor K_{root} was vulnerable (dark blue lines). The inset in C shows cumulative water-use efficiency (WUE; calculated as $A_{n,\,tot}$ over total transpiration rate) over time. Scenarios including a vulnerable K_{leaf} showed leaves that showed highest water-use efficiency, $A_{n,\,tot}$, and survived longer under drought conditions.

xylem conduit collapse in higher order veins, we tested the potential effect of the collapse of minor veins on K_{leaf} using a spatially explicit model of the leaf vein system. These simulations suggested that if xylem conduit collapse in the tertiary and minor veins were to occur within the range of water potentials in which K_{leaf} declined, this collapse would have a quantitatively small effect (i.e. causing a less than 10% decline in K_{leaf} at −0.5 MPa). This finding was consistent with previous model results showing that an extreme collapse of minor veins would cause K_{leaf} to decline only by up to 4% for four diverse species (Scoffoni et al., 2017b). Previous studies found collapse of xylem conduits in pine needles and the minor veins of red oak leaves, but only past the turgor loss point, and suggested that this could act as a circuit breaker to protect the stem xylem from embolism formation (Cochard et al., 2004a; Zhang et al., 2016). An early decline in outside-xylem pathways would act in a similar way, hastening stomatal closure, before xylem collapse would occur (Scoffoni et al., 2017a; see below). Past the turgor loss point, the Arabidopsis leaf undergoes drastic shrinkage in area and thickness, and it is likely that xylem in the midrib and higher order veins would collapse, especially as the Arabidopsis xylem cell walls are helicoidal and consist mostly of thick primary walls (Fig. 8). Future studies are needed to investigate the collapse of xylem and its influence on the rehydration capacity of strongly dehydrated leaves.

Response of K_{leaf} to Dehydration and Coordination with Gas Exchange

In Arabidopsis, we did not observe any embolism in leaf xylem conduits prior to, or even moderately past, the point of stomatal closure and the turgor loss point. This finding is consistent with recent work on tomato

Downloaded from https://academic.oup.com/plphys/article/178/4/1584/6116813 by University of California, San Francisco user on 29 November 2022

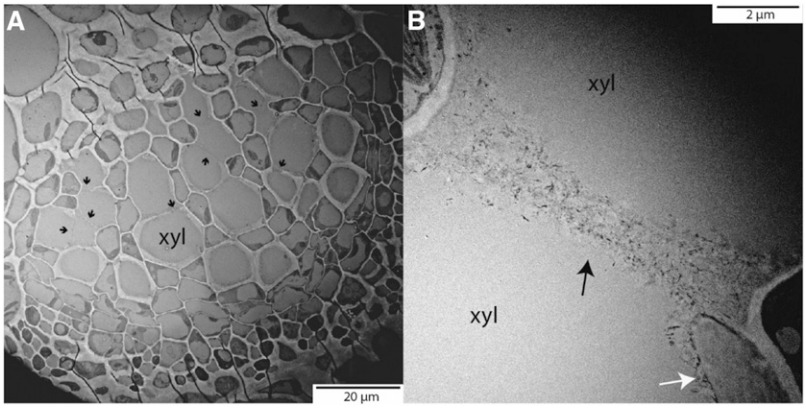

Figure 8. Transmission electron microscopy of Arabidopsis (Col-0) midrib cross sections. In A, the entire xylem (xyl) portion of the midrib can be seen. Black arrows point to the lack of secondary lignified wall around xylem conduits. These long primary wall sections can be observed in more detail in B. The white arrow points to a lignified portion of the secondary xylem wall. We hypothesize that the xylem resistance through these deeply helicoidal xylem conduits is reduced greatly, as unlignified primary cells effectively work as one large pit membrane.

(*Solanum lycopersicum*) and grapevine (*Vitis vinifera*) showing that stomata closed before any embolisms were observed using an optical visualization technique (Hochberg et al., 2017; Skelton et al., 2017). Here, we confirm this finding for the first time using microCT on Arabidopsis. This finding also is consistent with a growing body of literature showing that, typically, no xylem embolism is observed prior to the turgor loss point (Charra-Vaskou et al., 2012; Delzon and Cochard, 2014; Bouche et al., 2016; Brodribb et al., 2016b; Scoffoni et al., 2017a, 2017b). A recent study on sunflower (*Helianthus annuus*) showed that xylem embolism occurs after the turgor loss point even in plants that acclimate to drought: plants grown under water-limited conditions adjusted osmotically and had a more negative turgor loss point (−0.3 MPa shift), and leaf xylem P_{50} also shifted to a more negative value (−0.6 MPa shift; Cardoso et al., 2018).

The diurnal variation observed in g_s and net A_{area} was driven strongly by leaf water status (i.e. Ψ_{leaf}), as shown by our model-fitting analyses. Furthermore, our analyses indicated that the dynamics of Ψ_{leaf}, and thus of g_s and A_{area}, were driven strongly by the dehydration-induced decline of K_{leaf}, which resulted, in turn, from changes in outside-xylem pathways. Thus, we found that, in Arabidopsis, K_{leaf} declines more rapidly than g_s with dehydration, increasing the ratio of g_s to K_{leaf}, such that transpiration would amplify the decline in Ψ_{leaf} and, consequently, that of g_s. Indeed, 40% to 65% of the g_s decline was attributable to K_{leaf} decline for leaves dehydrated to less than 50% of stomatal closure. For more strongly dehydrated leaves, given their reduced g_s, the transpiration-driven amplification of Ψ_{leaf} and the g_s decline by K_{leaf} vulnerability are small, and declining Ψ_{leaf} due to low soil water potential and/or exogenous signals such as ABA or sugar production would be responsible for driving stomata to full closure. The direct mechanisms for stomatal closure with declining Ψ_{leaf} require further research. While most proximally, stomatal closure relates to solute transfer from guard cells to pavement cells, this could be driven by declining cell volume, turgor, osmotic concentration, or water potential, in the epidermis and/or mesophyll, partially or fully mediated by ABA accumulation, which, in turn, may be associated with declining cell volume and K_{leaf} decline in dehydrating leaves (McAdam and Brodribb, 2016; Sussmilch et al., 2017; Sack et al., 2018). Indeed, ABA signaling may contribute to stomatal closure both directly at the guard cells and also by contributing to K_{leaf} decline in dehydrating leaves by reducing cell membrane permeability in the bundle sheath and mesophyll via changes in aquaporin expression (Shatil-Cohen et al., 2011; Pantin et al., 2013). Indeed, our MOFLO 2.0 simulations showed that the K_{ox} decline was best explained by reduced cell membrane permeability and, to a lesser extent, cell connectivity. In Arabidopsis, stress-induced changes in cell membrane permeability, mediated by aquaporins, can have a strong impact on root hydraulic conductance (Javot and Maurel, 2002).

Alternatively, some studies have suggested that photosynthetic rate and carbon sink activities could regulate stomata and plant hydraulics (Nikinmaa et al., 2013; Körner, 2015; Rockwell et al., 2018). Indeed, this is well known in cropping systems such as grapevine, where the presence of strong sinks such as fruits have been shown to stimulate photosynthesis (Hofäcker, 1978; Petrie et al., 2000). Recent studies have found that excess cellular sugar concentrations under high irradiance, and/or during dehydration, could trigger stomata closure (Nikinmaa et al., 2013; Rockwell et al., 2018). Excess Suc may be transported to the guard cells by the transpiration stream, and the subsequent increase in osmolytes at the guard cell apoplast could induce stomatal closure in some species, especially during periods of high photosynthetic rates (Lu et al., 1995, 1997; Kang et al., 2007a, 2007b). Indeed, the increase in Suc concentration at the guard cells could act as more than a simple osmolyte, as it can depolarize the guard cell plasma membrane, activating potassium channels (Jarzyniak and Jasiński, 2014), and an increase in the level of sugar-sensing enzymes in the guard cells can accelerate stomatal closure by stimulating ABA production (Kelly et al., 2013; Van Houtte et al., 2013; Li et al., 2016, 2018; Medeiros et al., 2018). Additionally, excess Suc concentrations can decrease K_{ox}, and thus K_{leaf}, potentially via the deactivation of aquaporins (Kelly et al., 2017).

Downloaded from https://academic.oup.com/plphys/article/178/4/1584/6116813 by University of California, San Francisco user on 29 November 2022

In conclusion, K_{leaf}, g_s, and A_{area} show a coordinated decline during leaf dehydration in Arabidopsis, with a potentially strong direct effect of declining K_{leaf} in inducing stomatal closure via a decrease in water potential. The decline in K_{leaf} and g_s may be driven jointly by the accumulation of sugar and/or ABA accumulation in dehydrating leaves, or K_{leaf} declines may contribute to this accumulation. Future studies are needed to decipher the exact sequence of events leading stomata to close.

Putative Role of K_{ox} Decline in Improving Plant Carbon Balance, Water-Use Efficiency, and Survival during Drought

Why would the water transport pathways outside the xylem decline in efficiency during dehydration prior to the turgor loss point if this reduces gas exchange? Results from SurEau simulations indicated that a vulnerable K_{ox} (and thus K_{leaf}) above the turgor loss point leads to greater water-use efficiency and $A_{n,tot}$ as well as the protection of xylem from embolism and increased plant survival during drought. Simulated plants with K_{ox} declining prior to the turgor loss point operated, on average, at a lower K_{ox} value than plants with K_{ox} held constant (set to the average value measured at Ψ_{leaf} of -0.1 to -0.2 MPa [i.e. the range at which g_s was at its maximum]). This dynamic K_{ox} with water potential caused an up to 60% decline in g_s but only an up to 12% decline in CO_2 assimilation, resulting in a higher water-use efficiency and greater overall assimilation when considered over the entire period of soil drying. This benefit for low K_{ox} raises the question of why plants should invest in a high K_{ox} (or K_{leaf}) in maximally hydrated leaves. Indeed, high K_{leaf} values at Ψ_{leaf} above -1 MPa have at times been neglected when constructing vulnerability curves (Blackman et al., 2012, 2014) under the presumption that leaves simply do not operate at such high water potentials in planta. However, a high K_{ox} (and thus K_{leaf}) in well-hydrated leaves that declines during dehydration prior to the turgor loss point would offer advantages; it would enable high g_s and greater CO_2 assimilation under well-watered conditions. This would be particularly beneficial for a short-lived species such as Arabidopsis, which is required to grow rapidly when water availability is high. Previous studies have found that maximum K_{ox} (and K_{leaf}) was high and declined more rapidly with water potential in herbs (Scoffoni et al., 2011, 2017a; Nolf et al., 2016) than long-lived drought-tolerant chaparral trees (Scoffoni et al., 2017a). Ephemeral species such as Arabidopsis, or desert plants with short-lived leaves, would especially benefit from high CO_2 assimilation rates, and thus high K_{leaf} after a rainfall event, and gear down by reducing K_{leaf} and thus transpiration rates when water becomes scarce to improve their water-use efficiency and survive longer under soil drying (Grubb, 1998). In these simulations, root hydraulic vulnerability had a small effect on water-use efficiency in Arabidopsis. The much greater effect of leaf over root is due to the very high proportion of hydraulic resistance in the leaf (85.7%) due to the lack of stem in the vegetative phase of this rosette species. The hydraulic vulnerability of roots and their influence on the control of gas exchange are still under debate, given the experimental challenges. Debate is ongoing over whether root xylem is highly vulnerable (Hacke and Sauter, 1996; Hacke et al., 2000) or resistant (Rodriguez-Dominguez et al., 2018) to xylem embolism. However, just as in leaves (Scoffoni et al., 2017a), the root extra-xylem flow pathways might be more vulnerable. In grapevine, lacunae formation in fine root cortical cells may cause a strong decline in K_{root} under drying-soil conditions, which would help decouple the plant from drying soil and preserve its vascular system from embolism (Cuneo et al., 2016). Notably, plant competition for soil water is not simulated in the SurEau model. As such, we assume that plants have evolved to efficiently utilize soil water and not overspend it (Cowan, 1982; Buckley et al., 2017b).

The Light Response of K_{leaf} in Arabidopsis

Maximum K_{leaf} for well-hydrated leaves often increases in response to light; this response has been found for 15 of 30 species tested, in species of 23 plant families (Sack et al., 2002; Gasco et al., 2004; Tyree et al., 2005; Cochard et al., 2007; Scoffoni et al., 2008; Voicu et al., 2008; Guyot et al., 2012; Xiong et al., 2018). Furthermore, in some species, the light enhancement of K_{leaf} is reduced in dehydrated leaves, or, equivalently for those species, K_{leaf} declines with dehydration more steeply under high irradiance (Guyot et al., 2012). In Arabidopsis, a previous study suggested that the hydraulic conductance of entire rosettes had increased when acclimated to low rather than high irradiance (Prado et al., 2013). In our experiments using the evaporative flux method, we found significantly higher K_{leaf} values throughout the range of water potentials tested for leaves acclimated to high irradiance, with a 60% enhancement of K_{leaf} from low to high irradiance in well-hydrated leaves of Col-0. Discrepancies between these results may have arisen due to methodological differences, given that, in the study of Prado et al. (2013), hydraulic conductance was measured by pushing water inward through the stomata of entire rosettes suspended under water in darkness within a pressure chamber.

Notably, the light enhancement in K_{leaf} found in Arabidopsis did not result in a shift in P_{50}. This finding indicates a proportional shift to lower values under low irradiance, throughout the range of water potentials, contrary to findings for four woody species in which leaves acclimated to high irradiance were more vulnerable to K_{leaf} decline with dehydration (Guyot et al., 2012). The light enhancement of K_{leaf} would provide a greater hydraulic supply to meet the demand of leaves acclimated to high irradiance (i.e. given the strong and

Downloaded from https://academic.oup.com/plphys/article/178/4/1584/6116813 by University of California, San Francisco user on 29 November 2022

rapid dynamics of air temperature and humidity and wind), and thus higher VPD and leaf boundary layer conductance. Furthermore, given the strong transient dehydration during transpiration under these conditions, the higher K_{leaf} would contribute to rapid mesophyll rehydration at high water potential and thus enable the recovery of g_s and photosynthetic rate. The light enhancement of K_{leaf} could be caused by stronger temperature gradients throughout the leaf under high light and/or changes in aquaporin expression (Cochard et al., 2007). Our simulations of K_{ox} under low and high light using MOFLO 2.0 indicated that K_{leaf} would be minimally enhanced by temperature gradients in the leaf caused by light absorption, pointing to a role for aquaporins instead. This is consistent with the molecular evidence that aquaporin expression is sensitive to light (Cochard et al., 2007; Baaziz et al., 2012) and that multiple aquaporin isoforms are involved in a range of responses, such as K_{leaf} decline during drought and K_{leaf} light enhancement (Cochard et al., 2007; Pou et al., 2013; Laur and Hacke, 2014b, 2014a). Furthermore, aquaporins also may be involved in cell rehydration (Vitali et al., 2016). Finally, aquaporins also have been suggested to play a role in a rapid enhancement of K_{leaf} when Arabidopsis is suddenly exposed to low relative humidity, compensating for the increased evapotranspiration and allowing stomata to remain open (Levin et al., 2007).

Contribution of Hydraulic Traits to Arabidopsis Whole-Plant Physiology

Arabidopsis Col-0 has high values of K_{leaf}, g_s, and A_{area} relative to previously published values of diverse angiosperm species (Flexas et al., 2013; Scoffoni et al., 2017c) and displays strong sensitivity in K_{leaf} and gas exchange to dehydration. This physiological behavior is consistent with Arabidopsis' ruderal ecology, establishing and producing flowers and seeds in open or disturbed habitats in spring/early summer (Koornneef et al., 2004). The high values of K_{leaf} were driven by an especially high K_{ox} (106 mmol m^{-2} s^{-1} MPa^{-1}). This high K_{ox} is not untypical in herbs; in *Salvia canariensis*, maximum K_{ox} reached 231 mmol m^{-2} s^{-1} MPa^{-1} (Scoffoni et al., 2017a). Notably, high K_x, K_{ox}, and K_{leaf} often are achieved with allocation to substantial vein length per area, which increases flow paths in parallel within the xylem and reduces flow distance outside the xylem (Sack and Scoffoni, 2013); Arabidopsis possesses a relatively low vein length per area, but flow distance is strongly reduced by its very thin leaf, which also would reduce K_{ox} (Brodribb et al., 2007; Buckley et al., 2015). Furthermore, a high aquaporin activity and/or cell wall permeability, especially at the bundle sheath, could potentially influence K_{ox}; across several Arabidopsis mutants, maximum K_{leaf} was associated with an anatomical index of bundle sheath conductivity (Caringella et al., 2015). The high K_x value could potentially arise from the xylem structure (i.e. the numbers and sizes of xylem cells within minor veins; Caringella et al., 2015; Stewart et al., 2018) in combination with high conductance between xylem conduits. Indeed, our transmission electron microscopy imaging showed very little secondary lignification of xylem conduits throughout the midrib and other vein orders (Fig. 8), such that the bulk of midrib conduit walls are effectively one large pit membrane (i.e. primary unlignified wall) with water potentially leaking throughout the surface, a structure that would strongly reduce pit wall resistance and thus total xylem resistance (Choat et al., 2008).

Arabidopsis Col-0 also exhibits strong drought sensitivity, with its very low leaf mass per area (Wright et al., 2004), a very high degree of area shrinkage during dehydration (58% shrinkage when dry), high g_{min}, very high osmotic potential at full turgor, low modulus of elasticity and relative water content at the turgor loss point, and a turgor loss point that is among the highest values reported across angiosperm species (Bartlett et al., 2012), similar to that of the water potential at stomatal closure and at 88% loss of K_{leaf}, around −0.7 MPa. This detailed characterization of Arabidopsis Col-0 hydraulics traits, and their dynamics during leaf dehydration and implications for whole-plant responses, highlights useful avenues for high-throughput phenotyping and the elucidation of genetic mechanisms controlling these key traits, which would be loci for the manipulation of gas exchange and drought tolerance.

MATERIALS AND METHODS

Plant Material and Growth Conditions

Measurements were performed on Arabidopsis (*Arabidopsis thaliana* ecotype Col-0) plants grown continuously from December 2015 through November 2016. We grew Arabidopsis in a climate-controlled greenhouse at the University of California, Los Angeles. Seeds were sown in lawns in pots (3.13 inches wide × 4.88 inches long × 2.31 inches deep) in soil (1:1:2:1:1 mixture of washed plaster sand, loam, peat moss, perlite, and vermiculite) and cold acclimated at 4°C for 3 d in a chamber, then brought to the temperature-controlled greenhouse (minimum, mean, and maximum values for temperature, 19.3°C, 22.5°C, and 33.2°C; for humidity, 24%, 63%, and 92%; for irradiance [from 09:00 to 16:00], 11.2, 169, and 1,369 μmol photons m^{-2} s^{-1}). We recognize that many researchers often grow Arabidopsis in growth chambers under less than 300 μmol photons m^{-2} s^{-1} irradiance, and future work should consider the variation in leaf physiology, morphology, and anatomy driven by this lower irradiance. We chose to grow Arabidopsis in a greenhouse setting where plants are exposed to light fluctuations, with temporary high-light peaks, as is experienced in the field. Indeed, this has been shown to impact plant growth (Poorter et al., 2016). Furthermore, growing plants under such high irradiance means that these were not light limited; thus, our findings can be compared with those for other species grown without light limitation, as is typical in studies of plant hydraulic physiology.

When plants had true leaves after approximately 1 week, they were thinned to one individual per pot. Plants were watered regularly to keep soil moist. After approximately 6 weeks, at which point plants had more than 10 to 20 leaves, mature and healthy leaves were chosen for gas-exchange, hydraulic, and x-ray microCT measurements.

K_{leaf}

Pots were transported to the laboratory, watered, and enclosed overnight in plastic bags filled with wet paper towels to ensure a saturated atmosphere. To

Downloaded from https://academic.oup.com/plphys/article/178/4/1584/6116813 by University of California, San Francisco user on 29 November 2022

obtain a vulnerability curve spanning a range of Ψ_{leaf} values, well-hydrated and dehydrated leaves were measured. To obtain K_{leaf} values at high Ψ_{leaf}, mature and healthy leaves were cut directly at their base under water and their petioles were placed in a petri dish containing ultra-pure water (0.22-μm Thornton 200 CR; Millipore) prior to being connected to the evaporative flux system described below. To obtain K_{leaf} values at low Ψ_{leaf}, individuals were removed from the soil and dehydrated on the bench for 0.25 to 2 h, after which they were placed in bags which had previously been exhaled into, within a second bag filled with wet paper towels, to ensure high vapor and CO_2 concentration, to reduce stomatal opening and facilitate equilibration for 30 min. Two leaves then were measured for initial Ψ_{leaf}, using a pressure chamber (Plant Moisture Stress model 1000; PMS Instrument), with a grass fitting in the compression lid; for a few leaves with round petioles, silicon adaptors were used (Shatil-Cohen et al., 2011). On average, the two leaves measured for initial Ψ_{leaf} differed by 0.051 ± 0.008 MPa. A third mature and healthy leaf from the dehydrated individual was measured for K_{leaf}. After the leaf petiole was cut under water, it was gently wrapped with Parafilm and connected via tubing to a water source on a balance (±10 μg; models XS205 and AB265; Mettler Toledo), which logged the flow rate into the leaf every 5 s to a computer. The leaf was placed over a fan and under a light source (greater than 1,000 μmol m^{-2} s^{-1}; model 73828 1,000-W UV filter; Sears Roebuck). A water bath was placed between the leaf and the light to avoid overheating the leaf, which was kept between 23°C and 28°C as measured using a thermocouple (Cole-Parmer). After a minimum of 30 min to ensure light acclimation (Scoffoni et al., 2008) and once the flow had stabilized with no upward or downward trend, the average steady-state flow rate for the last 5 min was recorded and leaf temperature was measured (Cole-Parmer). The leaf was rapidly removed from the system, its petiole dabbed dry, and placed in a bag which had previously been exhaled into. The bagged leaf was placed into a second bag filled with wet paper towels and left to equilibrate for 30 min, after which final Ψ_{leaf} was measured. Leaf area was traced manually onto paper, scanned, and measured using ImageJ software (version 1.46r; National Institutes of Health). K_{leaf} was calculated as the flow rate divided by the Ψ_{leaf} driving force (the water potential of the water fed to the petiole [0 MPa] minus measured Ψ_{leaf}), normalized by leaf area and corrected for the dependence of water viscosity on temperature (to a reference value of 25°C; Weast, 1974; Yang and Tyree, 1993); this correction also approximately applies for the temperature dependence of vapor phase transport across this range of temperature (Buckley, 2015). Leaf hydraulic vulnerability curves were obtained as the plot of K_{leaf} versus the most negative Ψ_{leaf} experienced by the leaf (either the initial or final).

K_{leaf} vulnerability curves were measured under very low laboratory irradiance (light source off; less than 3 μmol photons m^{-2} s^{-1}) and high irradiance (greater than 1,000 μmol m^{-2} s^{-1}). Measurements in very low and high irradiance were performed on the same day using leaves taken from the same individuals when possible (i.e. when two leaves from the same individual were mature and healthy). Notably, the aim of this experiment was to test for a rapid light enhancement of K_{leaf} for high-light-grown individuals. Future studies are needed to investigate the plasticity in K_{leaf} and other physiological and morphological traits for Arabidopsis across different light growth regimes, as found to be important in a study of species of Hawaiian lobeliads (Scoffoni et al., 2015).

K_x

K_x was measured for six leaves (taken from six different individuals) using the vacuum pump method (Kolb et al., 1996; Nardini et al., 2001; Sack et al., 2004; Scoffoni and Sack, 2015; Trifiló et al., 2016). Briefly, individuals were rehydrated in the laboratory overnight and kept in dark plastic bags filled with wet paper towels to ensure high humidity. The next morning, a leaf was cut off the plant under ultra-pure water and placed in a petri dish over a white light transilluminator table (model TW; UVP) to allow visualization of the fourth-order veins (i.e. minor veins). Using a fresh scalpel, eight to 15 cuts per 1 cm^2 of leaf area were made to the lamina, severing minor veins, to ensure that outside-xylem pathways would be bypassed (Sack et al., 2004, 2005; Nardini and Salleo, 2005; Nardini et al., 2005b). Great care was taken to avoid cutting major veins; if they were cut by accident, the leaf was discarded. Once the cuts were made, the leaf petiole was wrapped with Parafilm and inserted through a small rubber stopper that had been perforated using a cork borer. The small rubber stopper then was connected to a tube fitting connected to silicone tubing (Cole-Parmer). The rubber stopper allowed a good seal around the petiole without crushing. We obtained a vacuum-tight seal by tightening the tubing around the rubber stopper with zipties and sealing the petiole to the exposed end of the rubber stopper using super glue (Loctite 409 glue; Henkel) with accelerator (Loctite 712 accelerator). Leaves were placed inside a vacuum flask with a thermocouple (Cole-Parmer) connected by a four-way valve to a vacuum pump (Gast) and a high-precision pressure gauge (±0.002 MPa; J4605 Marsh/Bellofram; Marshall Instruments).

We applied five increasing levels of partial vacuum, resulting in absolute pressures between 0.06 and 0.02 MPa, and recorded the flow rate of water entering the leaf from a water source on a balance (±10 μg; models XS205 and AB265; Mettler Toledo). The average flow rate of the last 5 min of stability for a given pressure was recorded, along with the temperature. The flow rate was normalized to 25°C, correct for the temperature response of the viscosity of water (Weast, 1974; Yang and Tyree, 1993). K_x was calculated as the slope of the flow rate versus pressure and normalized by leaf area, measured at the end of the experiment with a flatbed scanner. The percentage hydraulic resistance in the leaf xylem ($\%R_x$) and outside xylem ($\%R_{ox}$) were calculated as:

$$\%R_x = \frac{1/K_x}{1/K_{leaf}} \times 100 \quad (1)$$

$$\%R_{ox} = 100 - \%R_x \quad (2)$$

Diurnal Measurements of g_s, Photosynthetic Rate, and K_{plant} as a Function of Ψ_{leaf}

Diurnal measurements of light-saturated A_{max} and g_s were performed in the greenhouse on 40 individuals on November 11, 2016, from 9:00 to 18:00 using a portable gas-exchange system (LI-6400; LI-COR). The chamber CO_2 was set at 400 ppm. Because resolution was not sufficient to determine whether conduit collapse occurred in higher order veins, we simulated the potential impact of such a collapse if it had occurred. These simulations showed that, if higher order veins were to collapse to the same percentage of conduit diameter as reported recently for minor veins of $^{-2}$ s^{-1} photosynthetically active radiation, and leaf-to-air VPD was maintained between 0.4 and 0.6 kPa. Measurements were taken after the leaf had equilibrated in the chamber for 10 min; A_{max} and g_s were logged five times at 10-s intervals, and these five measurements were averaged. We checked that 10 min was sufficient equilibration time; $n = 7$ leaves were kept in the chamber for an additional 5 min; no significant differences were found between values taken at 10 min versus those taken at 15 min (paired Student's t test, $P = 0.08$). To verify g_s measurements, additional measurements were taken using a porometer on the abaxial side of the leaf (Delta-T Devices) on November 11, 2016, from 9:00 to 18:00. As expected, the g_s values obtained from the LI-COR device and porometer were within the same range of values and thus were pooled together during the analyses.

At the end of the measurement, the leaf was excised with a razor blade and immediately placed in a sealable bag (Whirl-Pak; Nasco), which had previously been exhaled into, and the bagged leaves were placed in a second bag filled with wet paper towels. After at least 30 min of equilibration, Ψ_{leaf} was measured using a pressure chamber as described above.

K_{plant} (mmol m^{-2} s^{-1} MPa^{-1}) was estimated under the assumption that soil water potential was fully saturated throughout the day (thus, $\Psi_{soil} = 0$ MPa). Although we did not measure Ψ_{soil} directly, plants were well watered and soil was always moist. Thus, K_{plant} was determined from the g_s obtained from the porometer data described above (measurements performed under ambient light irradiance), ambient VPD at the time of measurement, and Ψ_{leaf}:

$$K_{plant} = \frac{g_s \times VPD}{\Psi_{soil} - \Psi_{leaf}} \quad (3)$$

X-Ray MicroCT

To visualize leaf vein xylem embolism and tissue shrinkage, we used x-ray microCT at the synchrotron at the Advanced Light Source in Berkeley, California (Beamline 8.3.2). We imaged the xylem within the midrib and lamina tissues in 18 leaves of a range of Ψ_{leaf} values from nine individuals in February 2016 at 1.27-μm resolution. Three additional individuals were further scanned in November 2016 at a higher resolution of 0.638 μm to check for potential collapse in xylem conduits of the midrib. Arabidopsis individuals grown as described above were transported as carry-on in a plane to the Advanced Light Source. Individuals were fully rehydrated at the start of the experiment, whole plants were removed from the soil and dehydrated on the bench for different times to obtain a range of water potentials and equilibrated in double-sealed plastic bags for 30 min, after which two leaves were excised to obtain initial

Downloaded from https://academic.oup.com/plphys/article/178/4/1584/6116813 by University of California, San Francisco user on 29 November 2022

Ψ_{leaf}. Two of the leaves remaining attached to the plant were juxtaposed within a Styrofoam holder, and 0.653- to 0.869-mm-length scans were made of their midrib and surrounding lamina at the center of each leaf. A small piece of copper wire was attached at the center of the leaves to help center the samples for scanning. Kapton tape (DuPont) was used to tape the leaves and the copper wire to the Styrofoam holder to minimize sample movement during the scan. The Styrofoam with the sample enclosed was placed in a plexiglass cylinder, attached to a custom-built aluminum sample holder mounted on an air-bearing stage, and wet paper towels were placed above the sample in the plexiglass cylinder to minimize evaporation during the measurement. At the end of the measurement, final Ψ_{leaf} was recorded and leaf areas were measured. No significant differences in water potential before and after the measurement were observed (paired Student's t test, $P = 0.7$; $n = 8$). Scans were made at 20 to 23 keV in the synchrotron x-ray beam, and samples were rotated 180° with the instrument to enable visualization of the full 3D internal structure of the leaf. Scans took 5 to 10 min to complete, depending on the scan area selected. 3D volume renderings were made using the AVIZO 8.1.1 software (VSG) and used to count the number of embolized conduits in the entire sample and different vein orders. For the four samples that showed embolism, we measured the length of the embolized conduit and the widths of both conduit axes at three locations along the sample length. We also visualized for each section the water-filled conduits within the midrib and secondary veins to observe any potential deformation or collapse.

Using ImageJ software (version 1.46r; National Institutes of Health), we measured lamina tissue and cell dimensions on three cross-sectional images randomly selected in the middle of each sample. For each image, we measured the thickness of the lamina and of each tissue (i.e. the abaxial and adaxial epidermises, including the cuticle, and the palisade and spongy mesophyll) at three locations within the sample. We also measured the area, perimeter, and diameters as well as the percentage intercellular airspace of palisade and spongy mesophyll cells.

Drought Tolerance Traits

The leaf turgor loss point, osmotic potential at full turgor, relative water content at the turgor loss point, and modulus of elasticity were calculated from a pressure-volume curve constructed using 29 leaves from 20 individuals previously rehydrated overnight (Supplemental Fig. S3). Initial leaf mass was obtained for each single leaf before dehydration to a range of Ψ_{leaf}. Ψ_{leaf} values were measured with a pressure chamber after 30 min of equilibration in bags with high humidity, after which the leaf mass was measured again, along with leaf area, before it was placed in a drying oven at 70°C and measured for dry mass after 72 h. Pressure-volume curve parameters were obtained following standard protocols (Sack, 2010).

We measured the g_{min} (i.e. cuticular plus residual stomatal conductance) on nine mature leaves from nine individuals in June 2016 by following a standard protocol (Sack and Scoffini, 2010). Individual leaves were rehydrated covered in plastic in the laboratory the night before measurements. The next day, nine leaves were excised, their cut petioles were sealed with wax, and their fresh mass and leaf area were measured, before dehydration for 1 h taped to a fishing line above a fan, to ensure stomatal closure. Leaves were then repeatedly taken off the fan, bagged, and measured for mass every 20 min. After eight measurements were obtained for a given leaf, its area was measured again. The g_{min} was calculated as the slope of mass over time divided by the average mole fraction VPD during the measurement and normalized by the average of the initial and final leaf areas given shrinkage with dehydration during measurement. VPD was calculated from the temperature and relative humidity measurements obtained from a weather station (HOBO Micro Station with Smart Sensors; Onset). Finally, each individual leaf was dried in an oven at 70°C for 3 d, and dry mass and area were obtained to calculate leaf dry mass per hydrated area (in g m^{-2}) and the percentage area shrinkage in the dried leaf relative to the hydrated leaf.

Leaf Anatomy

Data for leaf venation and leaf cross-sectional anatomy of Col-0 to aid with the interpretation of microCT images were obtained from a previous study (Caringella et al., 2015).

To visualize xylem conduit walls, transmission electron microscopy was performed on three leaves from three Col-0 individuals in Germany. Small samples (approximately 2 mm wide and 8 mm long) from leaf midribs (and surrounding mesphyll) were cut under water and fixed in glutaraldehyde (2.5% glutaraldehyde, 0.1 mol of phosphate, and 1% saccharose, pH 7.3) overnight. After being washed in phosphate buffer and postfixed with 2% OsO_4, samples were dehydrated in a series of propanol solutions (30%, 50%, 70%, 90%, and three times 100%). Samples were finally immersed in 1.2-propylenoxide (CAS-no. 75.56-9), embedded gradually in Epon resin (Sigma-Aldrich), and polymerized at 60°C for 48 h. Ultrathin sections (less than 90 nm thick) were made with a Leica Ultracut UTC microtome (Leica Microsystems) and placed on copper slot grids. Observations were made using a JEOL 1400 transmission electron microscope at an accelerating voltage of 120 kV. Images were taken with a digital camera (Soft Imaging System).

Modeling of Hydraulic Function across Scales from Tissues to Whole Plants

We applied a framework of four models across scales to compute the mechanisms underlying K_{leaf} decline inside and outside the xylem, the causal role of K_{leaf} decline in driving stomatal closure, and the implications for gas exchange under simulated drought regimes (Table 1).

We first estimated the causal importance of mechanistic drivers of K_{leaf} decline using spatially explicit models of the leaf veins (K_LEAF; Cochard et al., 2004b; Scoffoni et al., 2017b) and outside-xylem pathways (MOFLO 2.0; Buckley et al., 2017a). Using K_LEAF, we tested whether xylem embolism and/or conduit collapse could explain the observed decline in K_{leaf}. We first tested for the impact of the embolisms observed with microCT imaging in the midrib and secondary veins on K_x and ultimately K_{leaf} (for more information on model parameterization, see Supplemental Methods; Supplemental Table S2). We tested the potential effect of the collapse of tertiary and minor vein conduits on K_x under two scenarios: (1) a realistic impact of conduit collapse on conduit conductivity (13% decline in tertiary and minor vein conductivity, similar to that observed in *Quercus rubra* [*Quercus rubra*] at the turgor loss point by Zhang et al. [2016]), and (2) a more severe conduit collapse scenario that would induce a 50% decline in tertiary and minor vein conduit conductivity (Supplemental Methods). Using MOFLO 2.0, we investigated the potential drivers of decline in K_{ox} with dehydration. We simulated the impact of an 80% decline in cell membrane permeability and/or a decline in cell-to-cell liquid phase hydraulic connectivity given the anatomical changes due to cell shrinkage at −0.5 MPa under different scenarios: (1) with or without an apoplastic barrier to liquid-phase water transport across the bundle sheath, and (2) under either no light or with an irradiance of 600 μmol m^{-2} s^{-1} photosynthetically active radiation to clarify a potential role of transdermal temperature gradients (Supplemental Methods; Supplemental Table S2).

We then quantified the direct influence of K_{leaf} decline on g_s decline with dehydration using a partitioning approach. We first considered the empirical maximum likelihood functions relating K_{leaf} and g_s to Ψ_{leaf}:

$$g_s = -451 \times |\Psi_{leaf}| + 339 \quad (4)$$

$$K_{leaf} = 6.83 + 81.4\exp(-7.56 \times |\Psi_{leaf}|) \quad (5)$$

Ψ_{leaf}, in turn, is a function of g_s, K_{leaf}, soil water potential (Ψ_{soil}), and the water vapor mole fraction gradient (Δw):

$$\Psi_{leaf} = \Psi_{soil} - \Delta w \frac{g_s}{K_{leaf}} \quad (6)$$

As Ψ_{leaf} declines during leaf dehydration, the resulting declines in g_s and K_{leaf} lead to changes in their ratio, g_s/K_{leaf}. If K_{leaf} declines more rapidly than g_s with Ψ_{leaf}, such that the ratio g_s/K_{leaf} increases, the decline in Ψ_{leaf} will be amplified, and consequently so will the decline in g_s itself. Therefore, K_{leaf} decline with dehydration would contribute to stomatal closure. The fraction of g_s decline with Ψ_{leaf} that can be attributed to K_{leaf} decline, F, is:

$$F = \frac{\frac{\partial g_s}{\partial K_{leaf}} \frac{\partial K_{leaf}}{\partial \Psi_{leaf}}}{\frac{\partial g_s}{\partial \Psi_{leaf}}} \quad (7)$$

where the partial derivative in the numerator is the sensitivity of g_s to Ψ_{leaf} with Ψ_{soil} and Δw held constant (1.5 kPa). That partial derivative is given by:

$$\frac{\partial g_s}{\partial K_{leaf}} = \frac{\partial g_s}{\partial \Psi_{leaf}} \cdot \frac{\partial \Psi_{leaf}}{\partial K_{leaf}} = \frac{\partial g_s}{\partial \Psi_{leaf}} \left[-\Delta w \left(\frac{1}{K_{leaf}} \frac{\partial g_s}{\partial K_{leaf}} - \frac{g_s}{K_{leaf}^2} \right) \right] \quad (8)$$

Downloaded from https://academic.oup.com/plphys/article/178/4/1584/6116813 by University of California, San Francisco user on 29 November 2022

Solving for $\partial g_s/\partial K_{leaf}$ gives:

$$\frac{\partial g_s}{\partial K_{leaf}} = \frac{\frac{\partial g_s}{\partial \Psi_{leaf}} \frac{g_s \Delta w}{K_{leaf}^2}}{1 + \frac{\partial g_s}{\partial \Psi_{leaf}} \frac{\Delta w}{K_{leaf}}} = \frac{\frac{\partial g_s}{\partial \Psi_{leaf}} \frac{g_s}{K_{leaf}}}{\frac{\partial g_s}{\partial \Psi_{leaf}} + \frac{K_{leaf}}{\Delta w}} \quad (9)$$

Combining Equations 7 and 9 gives F as:

$$F = \frac{\frac{\partial K_{leaf}}{\partial \Psi_{leaf}} \frac{g_s}{K_{leaf}}}{\frac{\partial g_s}{\partial \Psi_{leaf}} + \frac{K_{leaf}}{\Delta w}} \quad (10)$$

Finally, using a simplified discrete-time soil-plant hydraulic model (SurEau; Martin-StPaul et al., 2017), we estimated the influence of K_{leaf} decline on stomatal closure under varying simulations of soil and atmospheric drought. We simulated transpiration, g_s, cumulative photosynthetic rate, cumulative water-use efficiency, water potential, and PLC daily and during the course of soil drying until plant death (i.e., PLC = 100%). We performed these simulations following four different scenarios: (1) K_{leaf} and K_{root} were both vulnerable to dehydration prior to the turgor loss point (using the function of K_{leaf} versus Ψ_{leaf} measured with the EFM and the vulnerability of K_{root} obtained from that of K_{leaf} and K_{plant}, assuming no stem resistance in Arabidopsis; Supplemental Fig. S4); (2) K_{leaf} was vulnerable but not K_{root} (K_{root} was kept constant until xylem embolism occurred in the root); (3) K_{root} was vulnerable but not K_{leaf} (K_{leaf} was kept constant until xylem embolism occurred in the leaf); and (4) neither K_{leaf} nor K_{root} was vulnerable to dehydration (i.e. both K_{leaf} and K_{root} were kept at constant values until xylem embolism occurred; Supplemental Methods; Supplemental Table S3).

Statistics

We selected functions for the responses of K_{plant}, K_{leaf}, g_s, and A_{max} to Ψ_{leaf} using a maximum likelihood framework (Burnham and Anderson, 2002; Sack et al., 2006). For the g_s and A_{max} curve fitting, extremely low values at the beginning or end of the day, when stomata were shut in well-hydrated leaves ($\Psi_{leaf} > -0.01$ MPa), were discarded and likely represented the effects of the mechanical advantage of epidermal cells preventing stomatal opening in turgid leaves (Guyot et al., 2012); these points represented three of 63 and two of 26 of the points for g_s and A_{max}, respectively. We selected the maximum likelihood model using the optim function in R 3.4.1 (http://www.r-project.org). We fitted four types of functions to the curves, as used previously in the literature (Scoffoni et al., 2012), where Y = K_{leaf}, A_{area}, or g_s and Ψ_{leaf} is leaf water potential: linear ($Y = a\,\Psi_{leaf} + y_0$), two-parameter sigmoidal ($Y = a/(1 + e^{(-(\Psi leaf - x0)/b)})$), logistic ($Y = a/(1 + (\Psi_{leaf} / x_0)^b)$), and exponential ($Y = y_0 + a \times e^{-(b \times \Psi leaf)}$). We estimated the maximum Y value by extrapolating to $\Psi_{leaf} = 0$ and, as indices of decline with dehydration, the Ψ_{leaf} at which maximum Y values decreased by 50% and 95%. Because the best-fit function for the K_{leaf} vulnerability curve was exponential and the Y value at $\Psi_{leaf} = 0$ was extrapolated to a very high unrealistic value, we also estimated the maximum K_{leaf} by averaging all points above -0.1 MPa (K_{max}), as has been done typically in the literature (Sack et al., 2003; Nardini et al., 2005a; Brodribb and Jordan, 2008; Scoffoni et al., 2008, 2015).

To test for an effect of light on K_{leaf}, we selected the best-fit function for the response of K_{leaf} to Ψ_{leaf}, combining data for laboratory irradiance and high-irradiance treatments, using a maximum likelihood framework as explained above. We then calculated the residual variation for each leaf, subtracting the measured K_{leaf} (and irradiance) from the predicted K_{leaf} at the given Ψ_{leaf}, based on the best fit. We then performed Student's t test on the residuals obtained for the high- versus low-irradiance leaves across the entire range of Ψ_{leaf} as well as just for points above the turgor loss point and for well-hydrated leaves (above -0.2 MPa).

To determine the contribution of each correlated predictor variable (time, photosynthetically active radiation, temperature, VPD, and Ψ_{leaf}) to the observed variation in g_s diurnally, we applied independent effects analysis (Murray and Conner, 2009) using the hier.part function in R.3.4.1.

Supplemental Data

The following supplemental materials are available.

Supplemental Figure S1. External environmental drivers of g_s measured diurnally in a greenhouse with a porometer.

Supplemental Figure S2. Ψ_{leaf} is the main driver of observed diurnal variation in g_s.

Supplemental Figure S3. Pressure-volume curve for Arabidopsis (Col-0).

Supplemental Figure S4. Vulnerability curves of K_{plant}, K_{leaf}, and K_{root}.

Supplemental Table S1. K_LEAF simulation inputs.

Supplemental Table S2. Model inputs and simulation results from MOFLO 2.0.

Supplemental Table S3. SurEau inputs.

Supplemental Methods. K_LEAF, MOFLO, and SurEau simulations description.

ACKNOWLEDGMENTS

We thank Weimin Dang, Dula Parkinson, and Jessica Smith for technical assistance as well as the University of California, Los Angeles, Plant Growth Facility and the Advanced Light Source in Berkeley, California (Beamline 8.3.2).

Received June 18, 2018; accepted October 15, 2018; published October 26, 2018.

LITERATURE CITED

Baaziz KB, Lopez D, Rabot A, Combes D, Gousset A, Bouzid S, Cochard H, Sakr S, Venisse JS (2012) Light-mediated K(leaf) induction and contribution of both the PIP1s and PIP2s aquaporins in five tree species: Walnut (Juglans regia) case study. Tree Physiol **32:** 423–434

Bartlett MK, Scoffoni C, Sack L (2012) The determinants of leaf turgor loss point and prediction of drought tolerance of species and biomes: a global meta-analysis. Ecol Lett **15:** 393–405

Bartlett MK, Klein T, Jansen S, Choat B, Sack L (2016) The correlations and sequence of plant stomatal, hydraulic, and wilting responses to drought. Proc Natl Acad Sci USA **113:** 13098–13103

Blackman CJ, Brodribb TJ, Jordan GJ (2012) Leaf hydraulic vulnerability influences species' bioclimatic limits in a diverse group of woody angiosperms. Oecologia **168:** 1–10

Blackman CJ, Gleason SM, Chang Y, Cook AM, Laws C, Westoby M (2014) Leaf hydraulic vulnerability to drought is linked to site water availability across a broad range of species and climates. Ann Bot **114:** 435–440

Bouche PS, Delzon S, Choat B, Badel E, Brodribb TJ, Burlett R, Cochard H, Charra-Vaskou K, Lavigne B, Li S, et al (2016) Are needles of *Pinus pinaster* more vulnerable to xylem embolism than branches? New insights from X-ray computed tomography. Plant Cell Environ **39:** 860–870

Brodersen CR, McElrone AJ, Choat B, Lee EF, Shackel KA, Matthews MA (2013) In vivo visualizations of drought-induced embolism spread in *Vitis vinifera*. Plant Physiol **161:** 1820–1829

Brodribb TJ, Holbrook NM (2003a) Changes in leaf hydraulic conductance during leaf shedding in seasonally dry tropical forest. New Phytol **158:** 295–303

Brodribb TJ, Holbrook NM (2003b) Stomatal closure during leaf dehydration, correlation with other leaf physiological traits. Plant Physiol **132:** 2166–2173

Brodribb TJ, Holbrook NM (2004) Stomatal protection against hydraulic failure: A comparison of coexisting ferns and angiosperms. New Phytol **162:** 663–670

Brodribb TJ, Holbrook NM (2006) Declining hydraulic efficiency as transpiring leaves desiccate: Two types of response. Plant Cell Environ **29:** 2205–2215

Brodribb TJ, Holbrook NM (2007) Forced depression of leaf hydraulic conductance in situ: Effects on the leaf gas exchange of forest trees. Funct Ecol **21:** 705–712

Brodribb TJ, Jordan GJ (2008) Internal coordination between hydraulics and stomatal control in leaves. Plant Cell Environ **31:** 1557–1564

Brodribb TJ, Feild TS, Jordan GJ (2007) Leaf maximum photosynthetic rate and venation are linked by hydraulics. Plant Physiol **144:** 1890–1898

Brodribb TJ, Bienaimé D, Marmottant P (2016a) Revealing catastrophic failure of leaf networks under stress. Proc Natl Acad Sci USA **113:** 4865–4869

Downloaded from https://academic.oup.com/plphys/article/178/4/1584/6116813 by University of California, San Francisco user on 29 November 2022

Brodribb TJ, Skelton RP, McAdam SAM, Bienaimé D, Lucani CJ, Marmottant P (2016b) Visual quantification of embolism reveals leaf vulnerability to hydraulic failure. New Phytol **209:** 1403–1409

Bucci SJ, Scholz FG, Goldstein G, Meinzer FC, Sternberg LDL (2003) Dynamic changes in hydraulic conductivity in petioles of two savanna tree species: Factors and mechanisms contributing to the refilling of embolized vessels. Plant Cell Environ **26:** 1633–1645

Buckley TN (2015) The contributions of apoplastic, symplastic and gas phase pathways for water transport outside the bundle sheath in leaves. Plant Cell Environ **38:** 7–22

Buckley TN, John GP, Scoffoni C, Sack L (2015) How does leaf anatomy influence water transport outside the xylem? Plant Physiol **168:** 1616–1635

Buckley TN, John GP, Scoffoni C, Sack L (2017a) The sites of evaporation within leaves. Plant Physiol **173:** 1763–1782

Buckley TN, Sack L, Farquhar GD (2017b) Optimal plant water economy. Plant Cell Environ **40:** 881–896

Burnham KP, Anderson DR (2002) Model Selection and Multimodel Inference, Ed 2. Springer, New York

Cardoso AA, Brodribb TJ, Lucani CJ, DaMatta FM, McAdam SAM (2018) Coordinated plasticity maintains hydraulic safety in sunflower leaves. Plant Cell Environ **41:** 2567–2576

Caringella MA, Bongers FJ, Sack L (2015) Leaf hydraulic conductance varies with vein anatomy across *Arabidopsis thaliana* wild-type and leaf vein mutants. Plant Cell Environ **38:** 2735–2746

Carins Murphy MR, Jordan GJ, Brodribb TJ (2012) Differential leaf expansion can enable hydraulic acclimation to sun and shade. Plant Cell Environ **35:** 1407–1418

Charra-Vaskou K, Badel E, Burlett R, Cochard H, Delzon S, Mayr S (2012) Hydraulic efficiency and safety of vascular and non-vascular components in Pinus pinaster leaves. Tree Physiol **32:** 1161–1170

Choat B, Cobb AR, Jansen S (2008) Structure and function of bordered pits: New discoveries and impacts on whole-plant hydraulic function. New Phytol **177:** 608–625

Choat B, Brodersen CR, McElrone AJ (2015) Synchrotron x-ray microtomography of xylem embolism in Sequoia sempervirens saplings during cycles of drought and recovery. New Phytol **205:** 1095–1105

Choat B, Badel E, Burlett R, Delzon S, Cochard H, Jansen S (2016) Noninvasive measurement of vulnerability to drought-induced embolism by x-ray microtomography. Plant Physiol **170:** 273–282

Cochard H, Froux F, Mayr S, Coutand C (2004a) Xylem wall collapse in water-stressed pine needles. Plant Physiol **134:** 401–408

Cochard H, Nardini A, Coll L (2004b) Hydraulic architecture of leaf blades: Where is the main resistance? Plant Cell Environ **27:** 1257–1267

Cochard H, Venisse JS, Barigah TS, Brunel N, Herbette S, Guilliot A, Tyree MT, Sakr S (2007) Putative role of aquaporins in variable hydraulic conductance of leaves in response to light. Plant Physiol **143:** 122–133

Cowan IR (1982) Water use and optimization of carbon assimilation. *In* OL Lange, CB Nobel, CB Osmond, H Ziegler, eds, Encyclopedia of Plant Physiology. 12B. Physiological Plant Ecology. Springer-Verlag, Berlin, pp 589–630

Cuneo IF, Knipfer T, Brodersen CR, McElrone AJ (2016) Mechanical failure of fine root cortical cells initiates plant hydraulic decline during drought. Plant Physiol **172:** 1669–1678

Delzon S, Cochard H (2014) Recent advances in tree hydraulics highlight the ecological significance of the hydraulic safety margin. New Phytol **203:** 355–358

Flexas J, Scoffoni C, Gago J, Sack L (2013) Leaf mesophyll conductance and leaf hydraulic conductance: an introduction to their measurement and coordination. J Exp Bot **64:** 3965–3981

Gasco A, Nardini A, Salleo S (2004) Resistance to water flow through leaves of *Coffea arabica* is dominated by extra-vascular tissues. Funct Plant Biol **31:** 1161–1168

Grubb PJ (1998) A reassessment of the strategies of plants which cope with shortages of resources. Perspect Plant Ecol Evol Syst **1:** 3–31

Guyot G, Scoffoni C, Sack L (2012) Combined impacts of irradiance and dehydration on leaf hydraulic conductance: Insights into vulnerability and stomatal control. Plant Cell Environ **35:** 857–871

Hacke U, Sauter JJ (1996) Drought-induced xylem dysfunction in petioles, branches, and roots of *Populus balsamifera* L. and *Alnus glutinosa* (L.) Gaertn. Plant Physiol **111:** 413–417

Hacke UG, Sperry JS, Pittermann J (2000) Drought experience and cavitation resistance in six shrubs from the Great Basin, Utah. Basic Appl Ecol **1:** 31–41

Hochberg U, Windt CW, Ponomarenko A, Zhang YJ, Gersony J, Rockwell FE, Holbrook NM (2017) Stomatal closure, basal leaf embolism, and shedding protect the hydraulic integrity of grape stems. Plant Physiol **174:** 764–775

Hofäcker W (1978) Investigations on the photosynthesis of vines influence of defoliation, topping, girdling and removal of grapes. Vitis **17:** 10–22

Jarzyniak KM, Jasiński M (2014) Membrane transporters and drought resistance: A complex issue. Front Plant Sci **5:** 687

Javot H, Maurel C (2002) The role of aquaporins in root water uptake. Ann Bot **90:** 301–313

Kang Y, Outlaw WH Jr, Andersen PC, Fiore GB (2007a) Guard-cell apoplastic sucrose concentration: A link between leaf photosynthesis and stomatal aperture size in the apoplastic phloem loader *Vicia faba* L. Plant Cell Environ **30:** 551–558

Kang Y, Outlaw WH Jr, Fiore GB, Riddle KA (2007b) Guard cell apoplastic photosynthate accumulation corresponds to a phloem-loading mechanism. J Exp Bot **58:** 4061–4070

Kelly G, Moshelion M, David-Schwartz R, Halperin O, Wallach R, Attia Z, Belausov E, Granot D (2013) Hexokinase mediates stomatal closure. Plant J **75:** 977–988

Kelly G, Sade N, Doron-Faigenboim A, Lerner S, Shatil-Cohen A, Yeselson Y, Egbaria A, Kottapalli J, Schaffer AA, Moshelion M, et al (2017) Sugar and hexokinase suppress expression of PIP aquaporins and reduce leaf hydraulics that preserves leaf water potential. Plant J **91:** 325–339

Kolb KJ, Sperry JS, Lamont BB (1996) A method for measuring xylem hydraulic conductance and embolism in entire root and shoot systems. J Exp Bot **47:** 1805–1810

Koornneef M, Alonso-Blanco C, Vreugdenhil D (2004) Naturally occurring genetic variation in *Arabidopsis thaliana*. Annu Rev Plant Biol **55:** 141–172

Körner C (2015) Paradigm shift in plant growth control. Curr Opin Plant Biol **25:** 107–114

Laur J, Hacke UG (2014a) Exploring *Picea glauca* aquaporins in the context of needle water uptake and xylem refilling. New Phytol **203:** 388–400

Laur J, Hacke UG (2014b) The role of water channel proteins in facilitating recovery of leaf hydraulic conductance from water stress in *Populus trichocarpa*. PLoS ONE **9:** e111751

Levin M, Lemcoff JH, Cohen S, Kapulnik Y (2007) Low air humidity increases leaf-specific hydraulic conductance of Arabidopsis thaliana (L.) Heynh (Brassicaceae). J Exp Bot **58:** 3711–3718

Li Y, Xu S, Gao J, Pan S, Wang G (2016) Glucose- and mannose-induced stomatal closure is mediated by ROS production, Ca^{2+} and water channel in Vicia faba. Physiol Plant **156:** 252–261

Li Y, Xu S, Wang Z, He L, Xu K, Wang G (2018) Glucose triggers stomatal closure mediated by basal signaling through HXK1 and PYR/RCAR receptors in Arabidopsis. J Exp Bot **69:** 1471–1484

Lu P, Zhang SQ, Outlaw WH Jr, Riddle KA (1995) Sucrose: A solute that accumulates in the guard-cell apoplast and guard-cell symplast of open stomata. FEBS Lett **362:** 180–184

Lu P, Outlaw WH Jr, Smith BG, Freed GA (1997) A new mechanism for the regulation of stomatal aperture size in intact leaves (accumulation of mesophyll-derived sucrose in the guard-cell wall of *Vicia faba*). Plant Physiol **114:** 109–118

Martin-StPaul N, Delzon S, Cochard H (2017) Plant resistance to drought depends on timely stomatal closure. Ecol Lett **20:** 1437–1447

McAdam SAM, Brodribb TJ (2016) Linking turgor with ABA biosynthesis: Implications for stomatal responses to vapor pressure deficit across land plants. Plant Physiol **171:** 2008–2016

Medeiros DB, Perez Souza L, Antunes WC, Araújo WL, Daloso DM, Fernie AR (2018) Sucrose breakdown within guard cells provides substrates for glycolysis and glutamine biosynthesis during light-induced stomatal opening. Plant J **94:** 583–594

Murray K, Conner MM (2009) Methods to quantify variable importance: implications for the analysis of noisy ecological data. Ecology **90:** 348–355

Nardini A, Salleo S (2003) Effects of the experimental blockage of the major veins on hydraulics and gas exchange of *Prunus laurocerasus* L. leaves. J Exp Bot **54:** 1213–1219

Downloaded from https://academic.oup.com/plphys/article/178/4/1584/6116813 by University of California, San Francisco user on 29 November 2022

Nardini A, Salleo S (2005) Water stress-induced modifications of leaf hydraulic architecture in sunflower: Co-ordination with gas exchange. J Exp Bot **56:** 3093–3101

Nardini A, Tyree MT, Salleo S (2001) Xylem cavitation in the leaf of *Prunus laurocerasus* and its impact on leaf hydraulics. Plant Physiol **125:** 1700–1709

Nardini A, Gortan E, Salleo S (2005a) Hydraulic efficiency of the leaf venation system in sun- and shade-adapted species. Funct Plant Biol **32:** 953–961

Nardini A, Salleo S, Andri S (2005b) Circadian regulation of leaf hydraulic conductance in sunflower (*Helianthus annuus* L. cv Margot). Plant Cell Environ **28:** 750–759

Nikinmaa E, Hölttä T, Hari P, Kolari P, Mäkelä A, Sevanto S, Vesala T (2013) Assimilate transport in phloem sets conditions for leaf gas exchange. Plant Cell Environ **36:** 655–669

Nolf M, Rosani A, Ganthaler A, Beikircher B, Mayr S (2016) Herb hydraulics: inter- and intraspecific variation in three *Ranunculus* species. Plant Physiol **170:** 2085–2094

Pantin F, Monnet F, Jannaud D, Costa JM, Renaud J, Muller B, Simonneau T, Genty B (2013) The dual effect of abscisic acid on stomata. New Phytol **197:** 65–72

Petrie PR, Trought MCT, Howell GS (2000) Influence of leaf ageing, leaf area and crop load on photosynthesis, stomatal conductance and senescence of grapevine (Vitis vinifera L. cv. Pinot noir) leaves. Vitis **39:** 31–36

Pickard WF (1981) The ascent of sap in plants. Prog Biophys Mol Biol **37:** 181–229

Poorter H, Fiorani F, Pieruschka R, Wojciechowski T, van der Putten WH, Kleyer M, Schurr U, Postma J (2016) Pampered inside, pestered outside? Differences and similarities between plants growing in controlled conditions and in the field. New Phytol **212:** 838–855

Pou A, Medrano H, Flexas J, Tyerman SD (2013) A putative role for TIP and PIP aquaporins in dynamics of leaf hydraulic and stomatal conductances in grapevine under water stress and re-watering. Plant Cell Environ **36:** 828–843

Prado K, Boursiac Y, Tournaire-Roux C, Monneuse JM, Postaire O, Da Ines O, Schäffner AR, Hem S, Santoni V, Maurel C (2013) Regulation of Arabidopsis leaf hydraulics involves light-dependent phosphorylation of aquaporins in veins. Plant Cell **25:** 1029–1039

Rockwell FE, Gersony JT, Holbrook NM (2018) Where does Münch flow begin? Sucrose transport in the pre-phloem path. Curr Opin Plant Biol **43:** 101–107

Rodriguez-Dominguez CM, Buckley TN, Egea G, de Cires A, Hernandez-Santana V, Martorell S, Diaz-Espejo A (2016) Most stomatal closure in woody species under moderate drought can be explained by stomatal responses to leaf turgor. Plant Cell Environ **39:** 2014–2026

Rodriguez-Dominguez CM, Carins Murphy MR, Lucani C, Brodribb TJ (2018) Mapping xylem failure in disparate organs of whole plants reveals extreme resistance in olive roots. New Phytol **218:** 1025–1035

Sack L (2010) Leaf pressure-volume curve parameters. PrometheusWiki. http://www.publish.csiro.au/prometheuswiki/tiki-pagehistory.php?page=Leaf pressure-volume curve parameters&preview=10

Sack L, Holbrook NM (2006) Leaf hydraulics. Annu Rev Plant Biol **57:** 361–381

Sack L, Scoffoni C (2010) Minimum epidermal conductance (gmin a.k.a. cuticular conductance). PrometheusWiki. http://www.publish.csiro.au/prometheuswiki/tiki-pagehistory.php?page=Minimum epidermal conductance (gmin%2C a.k.a. cuticular conductance)&preview=

Sack L, Scoffoni C (2013) Leaf venation: Structure, function, development, evolution, ecology and applications in the past, present and future. New Phytol **198:** 983–1000

Sack L, Melcher PJ, Zwieniecki MA, Holbrook NM (2002) The hydraulic conductance of the angiosperm leaf lamina: A comparison of three measurement methods. J Exp Bot **53:** 2177–2184

Sack L, Cowan PD, Jaikumar N, Holbrook NM (2003) The 'hydrology' of leaves: co-ordination of structure and function in temperate woody species. Plant Cell Environ **26:** 1343–1356

Sack L, Streeter CM, Holbrook NM (2004) Hydraulic analysis of water flow through leaves of sugar maple and red oak. Plant Physiol **134:** 1824–1833

Sack L, Tyree MT, Holbrook NM (2005) Leaf hydraulic architecture correlates with regeneration irradiance in tropical rainforest trees. New Phytol **167:** 403–413

Sack L, Melcher PJ, Liu WH, Middleton E, Pardee T (2006) How strong is intracanopy leaf plasticity in temperate deciduous trees? Am J Bot **93:** 829–839

Sack L, John GP, Buckley TN (2018) ABA accumulation in dehydrating leaves is associated with decline in cell volume, not turgor pressure. Plant Physiol **176:** 489–495

Salleo S, Lo Gullo MA, Raimondo F, Nardini A (2001) Vulnerability to cavitation of leaf minor veins: any impact on leaf gas exchange? Plant Cell Environ **24:** 851–859

Scoffoni C, Sack L (2015) Are leaves 'freewheelin'? Testing for a wheeler-type effect in leaf xylem hydraulic decline. Plant Cell Environ **38:** 534–543

Scoffoni C, Pou A, Aasamaa K, Sack L (2008) The rapid light response of leaf hydraulic conductance: New evidence from two experimental methods. Plant Cell Environ **31:** 1803–1812

Scoffoni C, Rawls M, McKown A, Cochard H, Sack L (2011) Decline of leaf hydraulic conductance with dehydration: relationship to leaf size and venation architecture. Plant Physiol **156:** 832–843

Scoffoni C, McKown AD, Rawls M, Sack L (2012) Dynamics of leaf hydraulic conductance with water status: Quantification and analysis of species differences under steady state. J Exp Bot **63:** 643–658

Scoffoni C, Vuong C, Diep S, Cochard H, Sack L (2014) Leaf shrinkage with dehydration: Coordination with hydraulic vulnerability and drought tolerance. Plant Physiol **164:** 1772–1788

Scoffoni C, Kunkle J, Pasquet-Kok J, Vuong C, Patel AJ, Montgomery RA, Givnish TJ, Sack L (2015) Light-induced plasticity in leaf hydraulics, venation, anatomy, and gas exchange in ecologically diverse Hawaiian lobeliads. New Phytol **207:** 43–58

Scoffoni C, Chatelet DS, Pasquet-Kok J, Rawls M, Donoghue MJ, Edwards EJ, Sack L (2016) Hydraulic basis for the evolution of photosynthetic productivity. Nat Plants **2:** 16072

Scoffoni C, Albuquerque C, Brodersen CR, Townes ST, John GP, Bartlett MK, Buckley TN, McElrone AJ, Sack L (2017a) Outside-xylem vulnerability, not xylem embolism, controls leaf hydraulic decline during dehydration. Plant Physiol **173:** 1197–1210

Scoffoni C, Albuquerque C, Brodersen CR, Townes SV, John GP, Cochard H, Buckley TN, McElrone AJ, Sack L (2017b) Leaf vein xylem conduit diameter influences susceptibility to embolism and hydraulic decline. New Phytol **213:** 1076–1092

Scoffoni C, Sack L, Ort D (2017c) The causes and consequences of leaf hydraulic decline with dehydration. J Exp Bot **68:** 4479–4496

Shatil-Cohen A, Attia Z, Moshelion M (2011) Bundle-sheath cell regulation of xylem-mesophyll water transport via aquaporins under drought stress: A target of xylem-borne ABA? Plant J **67:** 72–80

Skelton RP, Brodribb TJ, Choat B (2017) Casting light on xylem vulnerability in an herbaceous species reveals a lack of segmentation. New Phytol **214:** 561–569

Stewart JJ, Polutchko SK, Demmig-Adams B, Adams WW III (2018) *Arabidopsis thaliana* Ei-5: Minor vein architecture adjustment compensates for low vein density in support of photosynthesis. Front Plant Sci **9:** 693

Sussmilch FC, Brodribb TJ, McAdam SAM (2017) Up-regulation of NCED3 and ABA biosynthesis occur within minutes of a decrease in leaf turgor but AHK1 is not required. J Exp Bot **68:** 2913–2918

Tixier A, Cochard H, Badel E, Dusotoit-Coucaud A, Jansen S, Herbette S (2013) *Arabidopsis thaliana* as a model species for xylem hydraulics: Does size matter? J Exp Bot **64:** 2295–2305

Trifiló P, Raimondo F, Savi T, Lo Gullo MA, Nardini A (2016) The contribution of vascular and extra-vascular water pathways to drought-induced decline of leaf hydraulic conductance. J Exp Bot **67:** 5029–5039

Tyree MT, Davis SD, Cochard H (1994) Biophysical perspectives of xylem evolution: Is there a tradeoff of hydraulic efficiency for vulnerability to dysfunction? IAWA J **15:** 335–360

Tyree MT, Nardini A, Salleo S, Sack L, El Omari B (2005) The dependence of leaf hydraulic conductance on irradiance during HPFM measurements: Any role for stomatal response? J Exp Bot **56:** 737–744

Van Houtte H, Vandesteene L, López-Galvis L, Lemmens L, Kissel E, Carpentier S, Feil R, Avonce N, Beeckman T, Lunn JE, et al (2013) Overexpression of the trehalase gene AtTRE1 leads to increased drought stress tolerance in Arabidopsis and is involved in abscisic acid-induced stomatal closure. Plant Physiol **161:** 1158–1171

Downloaded from https://academic.oup.com/plphys/article/178/4/1584/6116813 by University of California, San Francisco user on 29 November 2022

Vitali M, Cochard H, Gambino G, Ponomarenko A, Perrone I, Lovisolo C (2016) VvPIP2;4N aquaporin involvement in controlling leaf hydraulic capacitance and resistance in grapevine. Physiol Plant **158:** 284–296

Voicu MC, Zwiazek JJ, Tyree MT (2008) Light response of hydraulic conductance in bur oak (Quercus macrocarpa) leaves. Tree Physiol **28:** 1007–1015

Voicu MC, Cooke JEK, Zwiazek JJ (2009) Aquaporin gene expression and apoplastic water flow in bur oak (Quercus macrocarpa) leaves in relation to the light response of leaf hydraulic conductance. J Exp Bot **60:** 4063–4075

Wang X, Du T, Huang J, Peng S, Xiong D (2018) Leaf hydraulic vulnerability triggers the decline in stomatal and mesophyll conductance during drought in rice (Oryza sativa). J Exp Bot **69:** 4033–4045

Weast RC (1974) Handbook of Chemistry and Physics, Ed 54. CRC Press, Cleveland, OH

Wright IJ, Reich PB, Westoby M, Ackerly DD, Baruch Z, Bongers F, Cavender-Bares J, Chapin T, Cornelissen JHC, Diemer M, et al (2004) The worldwide leaf economics spectrum. Nature **428:** 821–827

Xiong D, Douthe C, Flexas J (2018) Differential coordination of stomatal conductance, mesophyll conductance, and leaf hydraulic conductance in response to changing light across species. Plant Cell Environ **41:** 436–450

Yang S, Tyree MT (1993) Hydraulic resistance in *Acer saccharum* shoots and its influence on leaf water potential and transpiration. Tree Physiol **12:** 231–242

Zhang YJ, Rockwell FE, Graham AC, Alexander T, Holbrook NM (2016) Reversible leaf xylem collapse: A potential "circuit breaker" against cavitation. Plant Physiol **172:** 2261–2274

Downloaded from https://academic.oup.com/plphys/article/178/4/1584/6116813 by University of California, San Francisco user on 29 November 2022